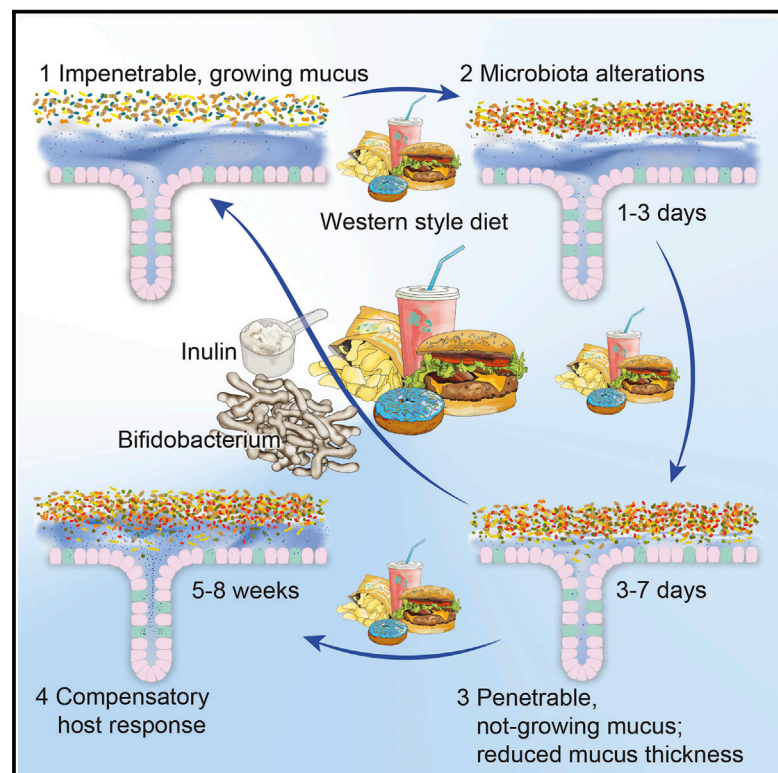


Cell Host & Microbe

Bifidobacteria or Fiber Protects against Diet-Induced Microbiota-Mediated Colonic Mucus Deterioration

Graphical Abstract



Authors

Bjoern O. Schroeder,
George M.H. Birchenough,
Marcus Ståhlman, Liisa Arike,
Malin E.V. Johansson,
Gunnar C. Hansson, Fredrik Bäckhed

Correspondence

gunnar.hansson@medkem.gu.se
(G.C.H.),
fredrik.backhed@wlab.gu.se (F.B.)

In Brief

The inner colonic mucus layer separates gut bacteria from their host. Schroeder et al. now find that gut bacteria can mediate functional defects of the mucus layer of mice fed a Western style diet. The defects can be prevented by application of a probiotic bifidobacteria or the prebiotic fiber inulin.

Highlights

- Western style diet impairs penetrability and growth of the colonic mucus layer in mice
- Mucus defects are accompanied by distinct alterations in microbiota composition
- Microbiota transplant from chow-fed mice prevents mucus aberrations in mice fed a WSD
- Mucus aberrations can be prevented by *Bifidobacterium longum* and inulin treatment



Bifidobacteria or Fiber Protects against Diet-Induced Microbiota-Mediated Colonic Mucus Deterioration

Bjoern O. Schroeder,¹ George M.H. Birchenough,² Marcus Ståhlman,¹ Liisa Arike,² Malin E.V. Johansson,² Gunnar C. Hansson,^{2,*} and Fredrik Bäckhed^{1,3,4,*}

¹Wallenberg Laboratory and Sahlgrenska Center for Cardiovascular and Metabolic Research, Department of Molecular and Clinical Medicine, Institute of Medicine, University of Gothenburg, 405 30 Gothenburg, Sweden

²Department of Medical Biochemistry, Institute of Biomedicine, University of Gothenburg, 405 30 Gothenburg, Sweden

³Novo Nordisk Foundation Center for Basic Metabolic Research, Section for Metabolic Receptology and Enteroendocrinology, Faculty of Health Sciences, University of Copenhagen, 2200 Copenhagen, Denmark

⁴Lead Contact

*Correspondence: gunnar.hansson@medkem.gu.se (G.C.H.), fredrik.backhed@wlab.gu.se (F.B.)

<https://doi.org/10.1016/j.chom.2017.11.004>

SUMMARY

Diet strongly affects gut microbiota composition, and gut bacteria can influence the colonic mucus layer, a physical barrier that separates trillions of gut bacteria from the host. However, the interplay between a Western style diet (WSD), gut microbiota composition, and the intestinal mucus layer is less clear. Here we show that mice fed a WSD have an altered colonic microbiota composition that causes increased penetrability and a reduced growth rate of the inner mucus layer. Both barrier defects can be prevented by transplanting microbiota from chow-fed mice. In addition, we found that administration of *Bifidobacterium longum* was sufficient to restore mucus growth, whereas administration of the fiber inulin prevented increased mucus penetrability in WSD-fed mice. We hypothesize that the presence of distinct bacteria is crucial for proper mucus function. If confirmed in humans, these findings may help to better understand diseases with an affected mucus layer, such as ulcerative colitis.

INTRODUCTION

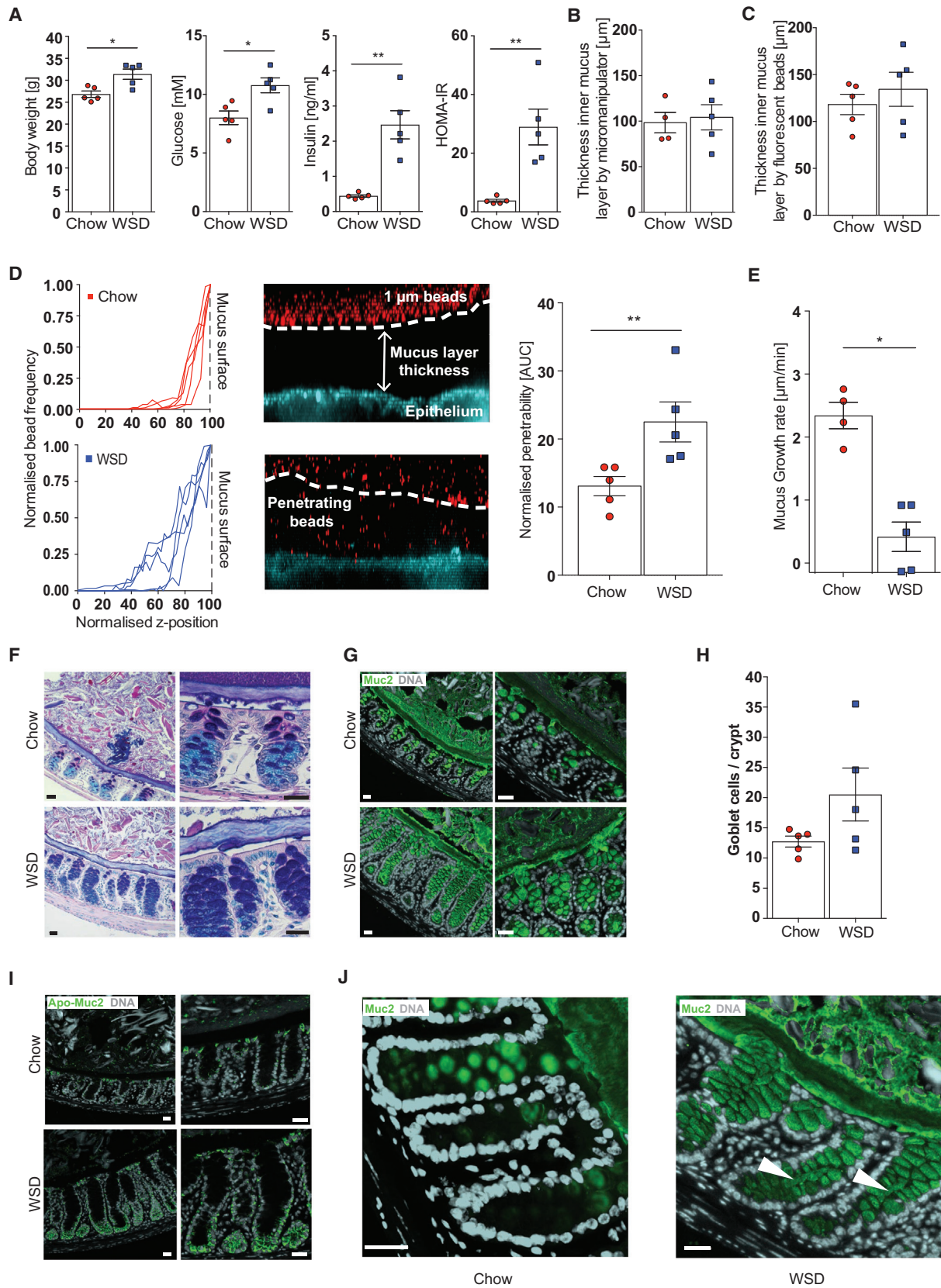
Colonic mucus is a physical barrier that consists of two layers and protects the host against the tremendous amounts of gut bacteria. In the healthy colon the inner layer is virtually sterile, well defined, and attached to the epithelium. In contrast, bacteria heavily colonize the outer mucus layer and degrade mucus glycans as an energy source (Johansson et al., 2008). Consequently, the outer layer is only loosely attached, less defined, and formed by mucus, bacteria, and intestinal content. Colonic mucus is maintained by an extensively glycosylated mucin-2 (Muc2) network, which expands after secretion from intestinal goblet cells and renews the inner mucus layer in 1–2 hr (Ambort et al., 2012; Johansson, 2012), thus preventing microbes from

reaching and translocating the intestinal epithelium (Johansson et al., 2008). Accordingly, structural defects or complete absence of the mucus layer can cause severe colitis in mice (Fu et al., 2011; Heazlewood et al., 2008; Johansson et al., 2008). In humans, similar bacterial penetration into the mucus layer was observed in patients with active ulcerative colitis (Johansson et al., 2014), and a correlation between mucus penetrability and dysglycemia has been observed (Chassaing et al., 2017).

Recent evidence has demonstrated that the intestinal microbiota can influence the properties of the colonic mucus layer (Earle et al., 2015; Jakobsson et al., 2015). Certain microbial generalists and specialists possess various carbohydrate utilization gene clusters that allow them to degrade and metabolize specific glycans of the intestinal mucus layer (Kaoutari et al., 2013; Martens et al., 2008). Indeed, bacterial glycan metabolism in mice that were colonized with 14 human gut microbiota species switched from fiber degradation to mucus glycan degradation when fed a fiber-free diet (Desai et al., 2016). Accordingly, feeding mice a fiber-depleted diet for up to 40 days reduced colonic mucus layer thickness, as analyzed in fixed tissue sections (Desai et al., 2016; Earle et al., 2015; Everard et al., 2013). Such a deteriorated colonic mucus layer contributed to lethal colitis when the mice were infected with the intestinal pathogen *Citrobacter rodentium* (Desai et al., 2016). Similarly, human obesity, which is often caused by high intake of a “Western style” diet (WSD), a diet rich in saturated fats and simple carbohydrates but depleted of dietary fiber, is a risk factor for infection by the enteric pathogen *Clostridium difficile* in humans (Bishara et al., 2013).

High intake of WSD is not only associated with obesity and metabolic disease, but also with an altered and less diverse gut microbiota composition (Cotillard et al., 2013; Filippo et al., 2010; Schnorr et al., 2014; Sonnenburg et al., 2016; Yatsunenkov et al., 2012). As the gut microbiota is a crucial environmental factor contributing to host physiology, alterations in their community composition change their metabolic output, which can affect nearby and distant organs in the host (Koh et al., 2016; Schroeder and Bäckhed, 2016). Moreover, metabolic disease can be initiated by microbial products, or potentially even intact





(legend on next page)

bacteria, translocating from the intestine into the systemic circulation (Burcelin et al., 2013; Caesar et al., 2012; Cani et al., 2007; Everard et al., 2013; Teixeira et al., 2012).

Although these observations indicate a defective mucosal barrier in obesity, it is at present unknown how WSD and obesity affect the intestinal mucus layer in living tissue. Thus, we here investigated the properties and function of the inner colonic mucus layer in mouse models of diet-induced and genetic obesity.

RESULTS

WSD Affects Growth Rate and Penetrability of the Colonic Mucus Layer

To explore how WSD affected the inner colonic mucus layer, we fed mice a WSD for 8 weeks and compared them with chow-fed littermates. As expected, consumption of WSD resulted in significantly higher body weight, fasting blood glucose, insulin levels, and homeostatic model assessment insulin resistance index (HOMA-IR) (Figure 1A), indicating a pre-diabetic state.

By using the *ex vivo* explant method (Gustafsson et al., 2012), in which intestinal content and the loosely attached outer mucus layer have been gently removed by flushing, we did not observe altered thickness of the inner mucus layer, either by measuring of the distance between the epithelium and 10 μm beads trapped on the mucus surface with a micromanipulator (Figure 1B) or by analyzing the distance between fluorescent 1 μm (bacteria-sized) beads and the stained epithelium with a confocal microscope (Figure 1C). However, we observed that penetrability of bacteria-sized beads into the mucus layer was greater in mice fed a WSD compared with chow-fed mice (Figure 1D; $p = 0.008$). Moreover, by taking thickness measurements over time we observed a significantly slower mucus growth rate ($p = 0.016$) in WSD-fed mice compared with chow-fed mice (Figure 1E).

To unravel whether the observed defective mucus layer is a consequence of dietary or host metabolic factors, we next studied mucus properties in leptin-deficient, genetically obese mice (Ob/Ob mice) that were fed a chow diet (Figure S1A). Blood glucose concentration in Ob/Ob mice is controlled by strongly augmented secretion of insulin, leading to a higher HOMA-IR. Mucus thickness was similar between Ob/Ob and lean mice (Figures S1B and S1C), but in contrast to the diet-induced obesity model, no significant difference in penetrability (Figure S1D) or

mucus growth rate (Figure S1E) was detected. Thus, our data suggest that WSD affects penetrability and growth rate of the inner colonic mucus and that the defects might be a consequence of dietary composition rather than of obesity and impaired glucose metabolism. However, since two out of six Ob/Ob mice displayed a highly penetrable inner mucus layer (Figure S1D) a diet-independent contribution to the phenotype cannot be excluded.

WSD Results in Increased Mucus Production

To evaluate whether the mucus phenotype can be explained by altered structural organization of the mucosal barrier, we stained Carnoy-fixed colonic tissue sections by Alcian blue/periodic acid-Schiff. A well-defined inner mucus layer and distinct dark-blue staining of mucus-producing goblet cells were observed in chow-fed mice (Figure 1F). In agreement with increased penetrability, the inner mucus layer appeared less organized upon WSD feeding. While some qualitative differences in the outer mucus layer were occasionally observed between chow- and WSD-fed mice, these are prone to artifacts from the diet composition and fixation procedure. We therefore limit our analysis to the inner mucus layer, which is well preserved and thus more reliable. Upon WSD feeding, the crypt goblet cells appeared more filled and intensely stained, an observation that was confirmed by staining for the Muc2 mucin (Figure 1G), and a trend toward increased number of goblet cells per crypt (Figure 1H). Increased penetrability of the mucus allows more bacteria to access the epithelium, which provokes several host responses, including faster turnover and production of the Muc2 mucin (Birchenough et al., 2016; Johansson et al., 2014). Indeed, we observed more intense staining for immature, non-O-glycosylated Muc2 at the bottom of the crypts in WSD-fed mice (Figure 1I). Secretion of the mature Muc2 is normally restricted to the crypt openings and epithelial surface; however, in WSD-fed mice Muc2 secretion was also observed along the entire length of the crypt (Figure 1J). We therefore conclude that impairment of the mucus barrier may provoke a compensatory host response.

WSD Does Not Alter Overall Mucus Protein Composition but Affects Distinct Proteins and Amount of Muc2

Evaluation of the mass spectrometry-based analysis of the mucus proteome revealed that WSD feeding did not cause any

Figure 1. Western Style Diet Feeding Impairs the Inner Colonic Mucus Layer in Mice

(A–C) Mice (4–5 mice/group) were fed a Western style diet (WSD) or chow diet for 8 weeks and metabolic parameters, such as body weight, fasting blood glucose, and insulin concentration, were measured, and HOMA-IR was calculated (A). Thickness of the inner colonic mucus layer was measured *ex vivo* with a micromanipulator by measuring the distance between black 10- μm beads and the epithelial surface (B) or with a confocal microscope by measuring the distance of fluorescent 1- μm (bacteria-sized) beads and the stained epithelium (C).

(D) Confocal z stacks (left), calculated from the position of fluorescent 1- μm beads (center), were used to determine penetrability of the inner colonic mucus layer (right). The median z stack is shown for each mouse. Fluorescent beads, inner mucus layer, and colonic epithelium are indicated in the figure. Turquoise, colonic tissue; red, bacteria-sized beads.

(E) Growth rate of the inner colonic mucus layer.

(F and G) Carnoy-fixed colonic tissue sections were stained with (F) Alcian blue/periodic acid-Schiff or with (G) polyclonal antibodies against glycosylated (mature) Muc2 (Muc2-C3, green). Please note that the outer mucus layer is less defined and often not observed in fixed tissue sections.

(H) Goblet cell number per colonic crypts.

(I and J) Carnoy-fixed colonic tissue sections (I) were incubated with polyclonal antibodies against non-O-glycosylated (immature) Muc2 (Muc2-PH497, green) and glycosylated (mature) Muc2 (Muc2-C3, green) (J). Arrows in (J) indicate mucus secretion inside the crypts.

Data in (A), (D), (E), and (H) are presented as means \pm SEM. Statistical significance was determined by Mann-Whitney U test with * $p < 0.05$ and ** $p < 0.01$. Scale bars, 25 μm ; representative images are shown. See also Figure S1.

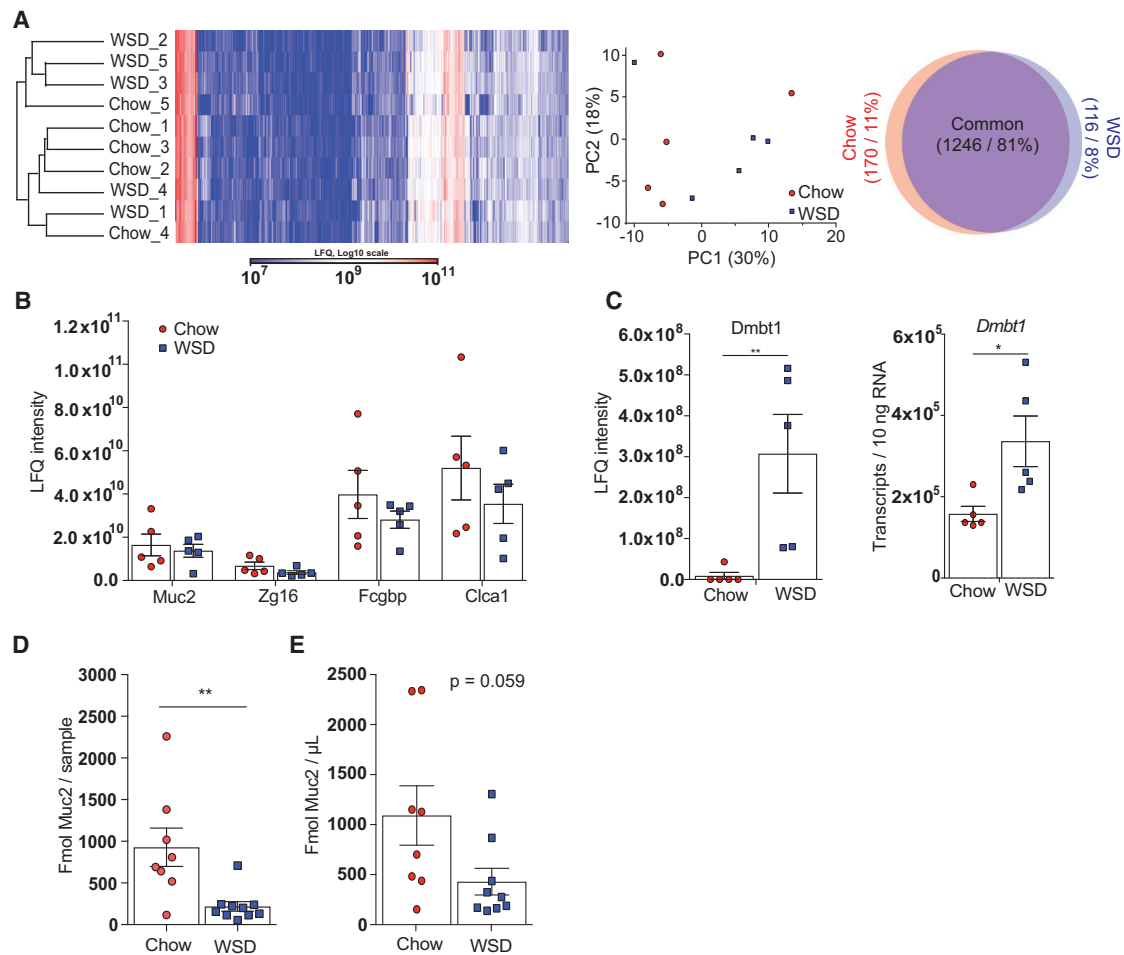


Figure 2. Western Style Diet Feeding Has a Minor Effect on the Mucus Proteome Composition but Provokes a Host Response

(A) Hierarchical clustering, principal component analysis, and Venn diagram of the mucus proteome from WSD- and chow-fed mice (n = 5 mice/group). Proteins that were detected in at least three samples per group are depicted in the Venn diagram.

(B) Label-free quantification (LFO) by mass spectrometry of the major mucus proteins Muc2, Zg16, Fcgbp, and Clca1 in colonic mucus.

(C) LFO of Dmbt1 protein in colonic mucus and its transcript quantification in colonic tissue.

(D and E) Absolute Muc2 protein quantification per sample (D) and normalized to volume (E) by mass spectrometry of Muc2 in the formed colonic mucus by using isotope-labeled Muc2 peptides (n = 8–10 mice/group).

Data are presented as means \pm SEM and statistical significance was determined by Mann-Whitney U test with * $p < 0.05$ and ** $p < 0.01$. In (C), Dmbt1 was below detection limit in four samples; those values were set to 0. See also [Figure S2](#) and [Table S2](#).

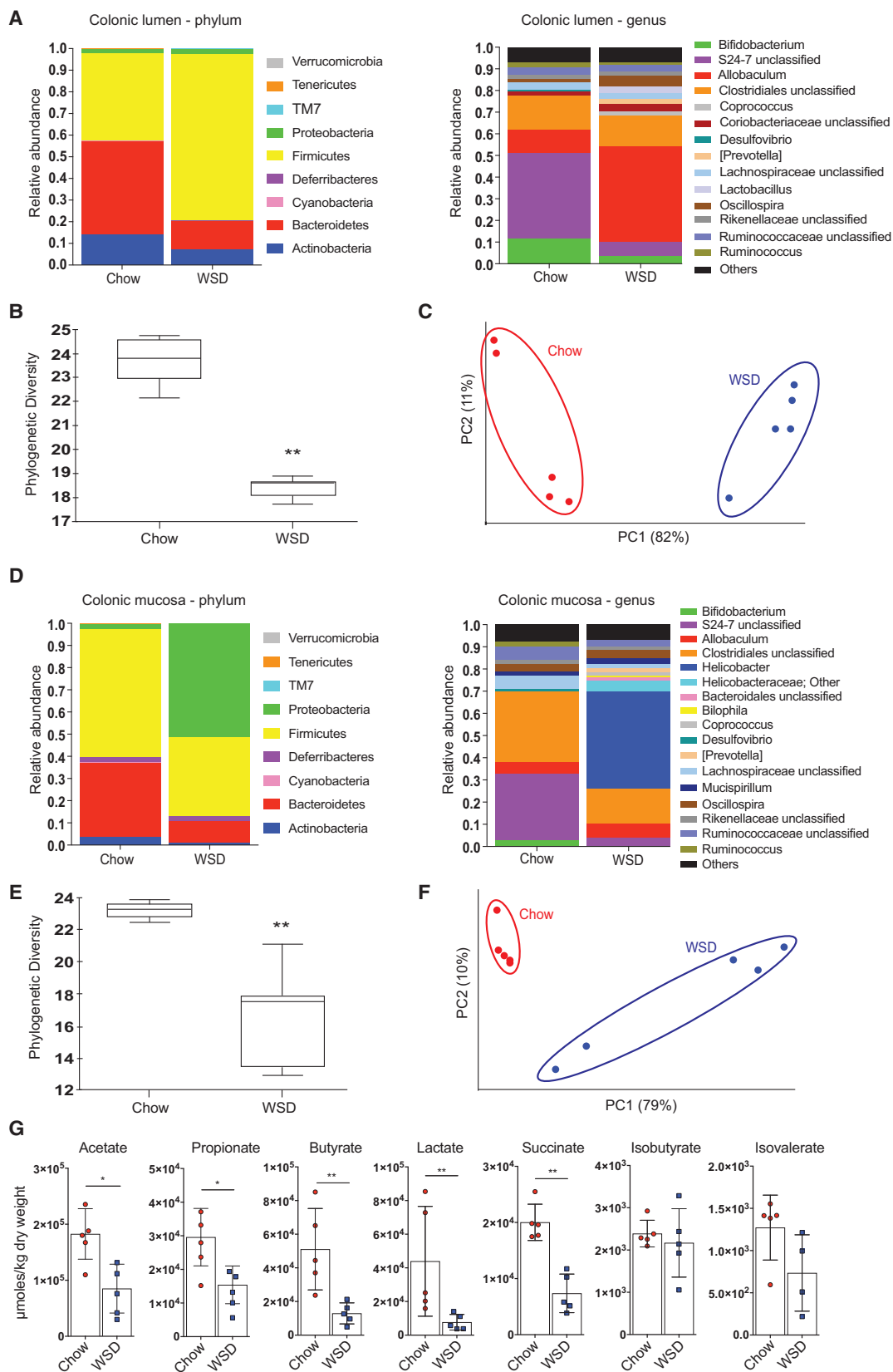
major global alteration in the mucus protein composition, as mucus samples were not separated based on diet in cluster analysis or principal component analysis ([Figure 2A](#)). Correspondingly, 81% of the proteins were detected in both dietary groups while 11% were unique to the chow group and 8% to the WSD group. Furthermore, according to mass spectrometry-based label-free quantification, no significant differences in relative protein abundance of the four major mucus proteins Muc2, Zg16, Fcgbp, and Clca1 were found between the two diet groups ([Figure 2B](#)). However, one protein, Dmbt1, demonstrated a large response to WSD ([Figure S2](#)). This protein can agglutinate bacteria and is thus involved in mucosal innate immunity ([Madsen et al., 2010](#)). The increased abundance of Dmbt1 in the mucus, as well as increased expression of *Dmbt1* in the colon of WSD-fed mice ([Figure 2C](#)), is possibly another element of the compensatory host response to the mucus

barrier defects and the subsequent contact of bacteria with the epithelium.

Absolute Muc2 quantification by using labeled standard peptides after *ex vivo* incubation revealed a significantly lower amount of Muc2 in mucus samples of WSD-fed mice compared with chow-fed mice ([Figure 2D](#)). Even though the difference in Muc2 concentration did not reach statistical significance ($p = 0.059$; [Figure 2E](#)), we hypothesize that the lower amount of Muc2 could result in a less dense mucus layer that might contribute to the higher penetrability observed in WSD-fed mice.

Luminal and Mucosal Distal Colonic Microbiota Are Altered in Mice Fed a WSD

Diet is a major factor modulating gut microbiota composition ([Cotillard et al., 2013](#); [David et al., 2014](#)), and we therefore investigated the gut microbiota composition by 16S rDNA analysis.



(legend on next page)

Similar to previous studies (Hildebrandt et al., 2009; Turnbaugh et al., 2008, 2009), we observed increased abundance of taxa belonging to Firmicutes and reduced abundance of Bacteroidetes and Actinobacteria in the colonic lumen of mice fed a WSD (Figure 3A; Table S1). At the genus level, the most pronounced alterations were the expansion of *Allobaculum* (44.2% versus 10.5%, $p < 0.001$, $p_{(adj)} < 0.05$), reduction of the S24-7 family (6.6% versus 39.5%, $p < 0.001$, $p_{(adj)} < 0.05$), and a reduction in *Bifidobacterium* genus (3.3% versus 11.6%, $p < 0.001$, $p_{(adj)} < 0.05$) in the WSD-fed mice. Moreover, feeding a WSD caused a significant reduction in α -diversity (Figure 3B; phylogenetic diversity whole tree, $p = 0.002$) and a significant separation of the microbial community (Figure 3C; weighted UniFrac, $p = 0.007$) from mice fed a chow diet.

Analysis of colonic mucosa-associated bacterial composition revealed a lower abundance of Bacteroidetes upon WSD feeding and a higher abundance of Proteobacteria (Figure 3D; Table S1), which was due to a bloom of the genus *Helicobacter* (43.7% versus 0.0%, $p < 0.001$, $p_{(adj)} = 0.06$). Furthermore, relative abundance of the S24-7 family (3.9% versus 29.6%, $p < 0.001$, $p_{(adj)} = 0.06$) and the *Bifidobacterium* genus (0.7% versus 2.9%, $p < 0.001$, $p_{(adj)} = 0.06$) was lower upon WSD feeding. In accordance with the luminal microbiota, we found a significantly lower α -diversity (Figure 3E; phylogenetic diversity whole tree, $p = 0.006$) and a clear separation of the microbial communities at the mucosa (Figure 3F; weighted UniFrac, $p = 0.003$).

The loss of potential fiber-degrading bacteria, such as the S24-7 family and *Bifidobacterium* (Kaoutari et al., 2013; Ormerod et al., 2016), is likely attributable to the lack of dietary fiber in the WSD. Dietary fiber is mainly fermented into short-chain fatty acids (SCFAs) by the gut microbiota. Consequently, SCFAs and other fermentation products were quantified to verify that microbial fiber metabolism was disrupted by WSD feeding. As expected, we observed significantly lower concentrations of the SCFAs acetate, propionate, and butyrate, as well as the organic acids lactate and succinate, in mice fed WSD (Figure 3G). In contrast, fermentation of branched chain amino acids was not altered, as indicated by similar levels of isobutyrate and isovalerate.

Shifts in Microbial Community Parallel Mucus Penetrability and Growth Defect

To investigate whether mucus growth defect and increased penetrability are linked to the alterations in the microbial community, we fed mice a WSD for up to 28 days ($n = 3$ mice per group and time point). We observed a rapid increase in body weight that plateaued after 7 days (Figure 4A) and a significant decrease in mucus thickness over the time course of the experiment (Figure 4B; $p = 0.002$), which has been observed previously when

feeding mice a fiber-free diet for 10–40 days (Desai et al., 2016; Earle et al., 2015; Everard et al., 2013). Regarding mucus properties and function, a significant reduction in mucus growth rate (Figure 4C; $p = 0.015$) and a significant increase in mucus penetrability ($p = 0.034$) were observed over the 28-day period, with both defects appearing between 3 and 7 days after initiation of WSD feeding (Figures 4D).

16S rDNA analyses from colonic luminal content (Figure 4E; Table S1) revealed a gradual decrease of Actinobacteria (*Bifidobacterium*), Bacteroidetes (family S24-7), Proteobacteria (*Sutterella*), and Verrucomicrobia (*Akkermansia*) between day 0 and 28, while Firmicutes (order Clostridiales, *Lactobacillus*, *Oscillospira*) increased in relative abundance. Due to blending of the fiber- and carbohydrate/fat-rich diets during the first day, α -diversity initially increased, but then decreased with prolonged WSD feeding (Figure 4F). Moreover, principal component analysis revealed significant clustering according to feeding duration (weighted UniFrac, $p = 0.001$; Figure 4G). Accordingly, reduction in mucus growth rate and increased penetrability co-occur between 3 and 7 days of WSD feeding, a time point when alterations in microbial composition have already started.

Examination of the mucosa over the course of the experiment (Figure 4H) revealed that the distinct goblet cell phenotype that was observed after prolonged WSD feeding (Figure 1F) was not fully developed after 28 days. This indicates that the goblet cell phenotype is not causative for growth defect and penetrability of the mucus layer but rather might be a consequence.

Microbiota Transplantation Prevents the Defect in Mucus Properties

To elucidate whether the gut microbiota is causal for the reduced mucus growth and increased penetrability, we performed a microbiota transplantation experiment (Figure 5A). After initial antibiotic treatment, mice received a weekly microbial transplant from either WSD-fed mice (WSD → WSD) or from chow-fed mice (WSD → Chow) while feeding on a WSD. Over the course of the experiment no difference in body weight was observed between the groups (Figure S3A). Likewise, when the experiment was terminated after 6 weeks we did not observe differences in metabolic parameters such as body weight, body fat, fasting blood glucose, fasting insulin concentration, or HOMA-IR (Figures 5B and S3B), or the length of the colon (Figure S3C). However, penetrability of the mucus layer was significantly lower in WSD → Chow mice in comparison with WSD → WSD mice (Figure 5C; $p = 0.009$). Similarly, growth of the inner colonic mucus layer was fully restored in WSD → Chow mice (Figure 5D; $p = 0.004$), while total mucus thickness was not significantly altered between the two groups (Figure S3D). Of note,

Figure 3. Microbiota Composition in the Colonic Lumen and at the Mucosa Is Altered in WSD-Fed Mice

Relative abundance of microbial taxa was determined by 16S rDNA analysis in the lumen (A–C) and at the mucosa (D–F) of the distal colon in WSD- and chow-fed mice ($n = 5$ mice/group).

(A) Relative abundance of luminal taxa was determined on phylum and genus level, for which abundances $>1\%$ are shown.

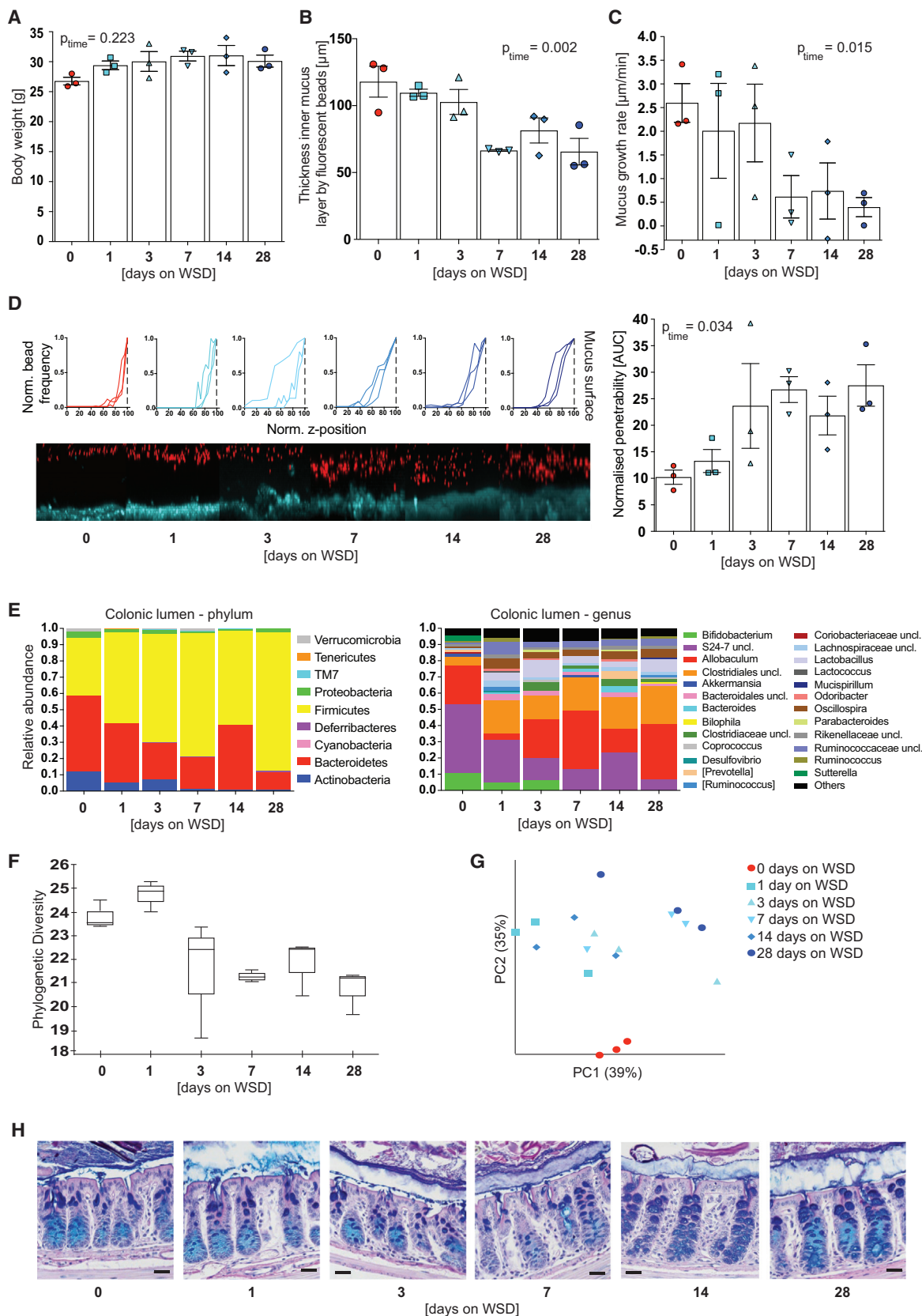
(B and C) α -Diversity (B) and β -diversity (weighted UniFrac) (C) for the luminal microbial community.

(D) Relative abundance of mucosa-associated taxa was determined on phylum and genus level, for which abundances $>1\%$ are shown.

(E and F) α -Diversity (E) and β -diversity (weighted UniFrac) (F) for the mucosa-associated microbial community. Statistical significance for diversity analyses was calculated as described in STAR Methods.

(G) Cecal fermentation products of mice fed WSD or chow diet determined by gas chromatography-mass spectrometry.

Data are presented as means \pm SEM and statistical significance was determined by Mann-Whitney U test with * $p < 0.05$ and ** $p < 0.01$. See also Table S1.



(legend on next page)

concentrations of cecal fermentation products were also similar in both mouse groups (Figure 5E), suggesting that the observed mucus defect may be independent of these microbial metabolites.

By 16S rDNA analysis in the colonic lumen, we identified lower abundance of Firmicutes and higher abundance of Bacteroidetes in WSD→Chow mice (Figure 5F; Table S1). Moreover, relative abundance of Bifidobacteria increased from 0.2% to 3.7% ($p < 0.001$, $p_{(adj)} < 0.05$) and S24-7 family from 6.3% to 16.2% ($p < 0.05$, $p_{(adj)} = 1.0$), while abundance of *Allobaculum* decreased from 36.4% to 16.3% ($p < 0.01$, $p_{(adj)} = 0.19$) upon receiving the WSD→Chow microbiota transplant. These alterations were accompanied by a significant re-gain in α -diversity (Figure 5G; phylogenetic diversity whole tree, $p = 0.018$) and a significant separation from mice receiving the WSD→WSD transplant (Figure 5H; weighted UniFrac, $p = 0.028$). Notably, the growth rate of the inner mucus layer correlated with relative abundance of *Bifidobacterium* while mucus penetrability displayed a threshold-like dependency (Figure S3E).

Bifidobacterium longum or Inulin Supplement Prevents Mucus Defects

Since the abundance of *Bifidobacterium* correlated with mucus growth rate (Figure S3E) and was dramatically reduced between 3 and 7 days of WSD feeding (Figure 4E), we tested whether *Bifidobacterium* was causally involved in colonic mucus properties. We thus fed mice a WSD for 4 weeks and supplemented their drinking water with either prebiotic oligofructose-enriched inulin, which is known to enrich bifidobacteria (Gibson et al., 1995; Rossi et al., 2005; Vandeputte et al., 2017); the probiotic strain *Bifidobacterium longum* NCC 2705 (*B. longum*); or with a synbiotic combination of both (Figure 6A). As higher concentrations of inulin have been described to improve metabolic dysfunction (Dewulf et al., 2011; Kumar et al., 2016), but our microbiota transplant experiment did not reveal any metabolic improvements (Figures 5B, S2A, and S2B), we provided inulin only at a low concentration (1%). Accordingly, supplementation of the probiotic, prebiotic, or synbiotic to the WSD did not lead to improved metabolic parameters in WSD-fed mice (Figure 6B). In contrast, supplementation with inulin was sufficient to prevent penetrability of the inner colonic mucus layer (Figures 6C and 6D; $p = 0.007$). However, this protective effect was not observed in mice receiving either *B. longum* or the synbiotic combination. Conversely, the mucus growth defect was prevented by *B. longum* in the absence ($p = 0.006$) or presence ($p = 0.005$) of inulin, but not by the prebiotic fiber inulin alone (Figure 6E). In agreement with our previous results, no alterations

in mucus thickness were observed by any of the treatments (Figure 6F). Accordingly, probiotic and prebiotic treatments can prevent individual but distinct aspects of the WSD-induced mucus defects. Significantly, these data thus indicate that the WSD-induced increase in mucus penetrability and decrease in mucus growth rate are not directly linked.

DISCUSSION

Here, we have shown that WSD-mediated alterations of the gut microbiota composition cause defects of the inner colonic mucus layer, which includes a strongly reduced growth rate and higher penetrability. We observed that a loss of *Bifidobacterium* taxa paralleled the onset of the mucus defects, and that mucus growth positively correlated with *Bifidobacterium* abundance. Consistently, supplementation of WSD with a *B. longum* strain prevented the growth defect, but not the increase in penetrability, which was instead prevented by the addition of inulin. Despite the co-occurrence of both phenotypes in our experiment involving full microbial communities, we deciphered that mucus penetrability and growth rate are separate events.

Diet rapidly affects gut microbiota composition, and mice fed a fiber-deficient diet over several generations exhibit a progressive loss in distinct taxa and microbial diversity (Cotillard et al., 2013; David et al., 2014; Sonnenburg et al., 2016). However, microbial changes caused by a lack of fiber occur rapidly (Turnbaugh et al., 2009), and we accordingly observed significantly decreased diversity and reduced abundance of Bacteroidetes and Actinobacteria when we switched mice to a low-fiber WSD. Importantly, the gut microbiome encodes a large variety of carbohydrate-active enzymes (Kaoutari et al., 2013) and, in the absence of dietary fiber, distinct microbial taxa can switch to host glycans of the intestinal mucus layer (Desai et al., 2016; Earle et al., 2015; Martens et al., 2008). We found that microbiota alterations and loss of diversity paralleled or even preceded the increase in mucus penetrability after changing from chow diet to WSD. While further studies are required to formally demonstrate microbial mucus degradation in a complex WSD-fed gut microbial community, it is likely that the increased penetrability is a consequence of the dietary shift of the microbial ecology and the subsequent altered microbial metabolism.

Previous studies (Desai et al., 2016; Earle et al., 2015; Everard et al., 2013) that evaluated mucus thickness in fixed tissue sections described thinner colonic mucus in mice that were fed low-fiber diets for short periods of time (10–40 days). Despite different methods, we also observed thinner mucus after 28 days

Figure 4. Mucus Penetrability and Growth Defect Co-occur and Are Accompanied by Distinct Alterations in Microbiota Composition

(A–C) After 0–28 days of WSD feeding, body weight (A), colonic mucus thickness (B), and colonic mucus growth rate (C) were determined from three mice per time point.

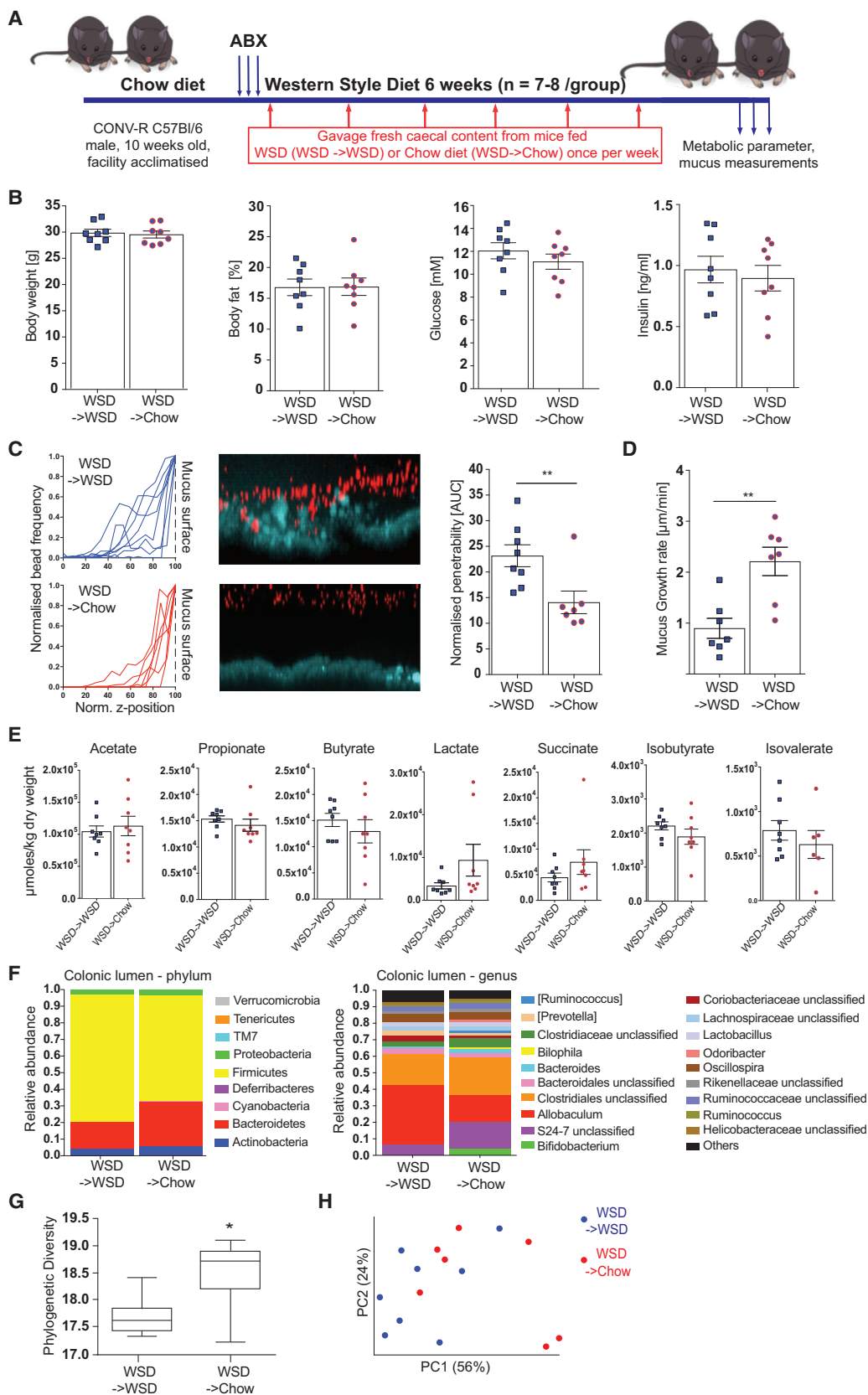
(D) Confocal z stacks were calculated from the position of fluorescent 1- μ m beads as shown and used to determine the normalized penetrability of the inner colonic mucus layer (right). The median z stack is shown for each mouse. Turquoise, colonic tissue; red, bacteria-sized beads.

Data in (A)–(D) are presented as mean \pm SEM and statistical significance was determined by linear regression over time.

(E) Relative abundance of luminal colonic bacteria was determined on phylum and genus level, for which abundances $>1\%$ are shown. Uncl., unclassified.

(F and G) α -Diversity (F) and β -diversity (weighted UniFrac) (G) for the colonic microbial communities. Statistical significance for diversity analyses was calculated as described in the STAR Methods.

(H) Carnoy-fixed colonic tissue sections were stained with Alcian blue/periodic acid-Schiff. Scale bars, 25 μ m; representative images are shown. See also Table S1.



(legend on next page)

of WSD feeding in our time course experiment. However, when feeding WSD for 8 weeks no difference in mucus thickness was observed when compared with chow-fed mice. It is thus possible that long-term WSD feeding leads to adaptational host processes that correct the initially reduced mucus thickness by a yet unknown mechanism.

Evaluation of mucus properties is challenging due to its composition and the factors that influence the mucus layer. This does not only include environmental factors such as pH, water content, and ion composition, but also amount and frequency of stool passages, food consistency, and motility of the gut. Moreover, tissue fixation by all fixatives causes significant mucus shrinkage due to its high water content, which may affect thickness measurements in fixed tissue sections (Desai et al., 2016; Earle et al., 2015; Everard et al., 2013). In contrast, *ex vivo* analyses, as described herein, provide important clues to mucus kinetics and quality, although some environmental cues may be different compared with the *in vivo* situation.

As a WSD-associated microbiota seemed responsible for our observed mucus defects, we reasoned that a fiber-associated community might be protective. Indeed, we found that microbiota transfer from chow-fed mice could correct the WSD-induced impairment of mucus physiology, yet without affecting host metabolic parameters. To examine which microbial taxa may confer the protective mucus effects we mined our microbiota data and observed that one of the most affected genera upon WSD was *Bifidobacterium*. Thus, we investigated whether bifidobacteria has a protective effect by treating mice with *B. longum* and/or the fiber inulin. We observed that, while *B. longum* administration corrected mucus growth, only inulin corrected mucus penetrability, suggesting that other inulin-responsive bacteria might be involved in this effect. Surprisingly, the synbiotic combination of *B. longum* and inulin did not significantly prevent penetrability of the inner mucus layer, even though inulin alone had a protective effect. We hypothesize that the supplemented *B. longum* community metabolizes parts of the provided inulin in the mouse gut, thus reducing the effective inulin concentration required to prevent mucus penetrability.

Bifidobacterium strains have long been used as probiotics (Picard et al., 2005) and have several beneficial effects, including preventing translocation of enteropathogenic *Escherichia coli* O157 in mice (Fukuda et al., 2011) and strengthening epithelial barrier function in human ulcerative colitis patients

(Duranti et al., 2016). Moreover, some *Bifidobacterium* strains can bind to mucus proteins *in vitro* (He et al., 2001). It is thus possible that *Bifidobacterium* species exert part of their probiotic action by stimulating colonic mucus growth. Importantly, prebiotic treatment with fiber does not only alter the abundance of *Bifidobacterium*, but more than 100 other bacterial taxa (Everard et al., 2011). Thus, the inulin-mediated effects may also be *Bifidobacterium* independent.

A recent study has found that a fiber-deprived synthetic microbiota comprised of 14 human gut bacterial species started to degrade host mucin glycans upon removal of fiber from the host diet, resulting in a thinner mucus layer (Desai et al., 2016). Supplementation of the fiber-free diet with purified soluble glycans (resembling prebiotic formulations) did not prevent the mucus alterations. A possible explanation is that the synthetic community, which is an excellent tool to study metabolic alterations of distinct sequenced community members (Desai et al., 2016; Martens et al., 2008; Sonnenburg et al., 2005), lacks important fiber-dependent bacteria that are beneficial for mucus function. Moreover, a synthetic community of human-adapted bacterial strains in mouse models may be insufficient to provoke an adequate immune response in the mouse gut (Chung et al., 2012). By using a natural and more complex mouse bacterial community we found that the defective mucus barrier causes a host defense response after long-term WSD feeding. This included increased cellular mucus production, mucus secretion into the crypts, and higher levels of Dmbt1. Such a compensatory response was absent in the synthetic community using a fiber-free diet (Desai et al., 2016), likely due to the reasons described above. However, since our diet included high amounts of fat and sucrose, a potential effect of these dietary compounds on the host tissue cannot be fully excluded.

In conclusion, we found that diet-mediated alteration of the gut microbiota led to rapid deterioration of the inner colonic mucus layer. As supplementation with probiotic bifidobacteria or prebiotic fiber prevented mucus defects, we hypothesize that the presence of distinct bacteria is crucial for proper mucus function. Modern diets such as WSD increase the risk for developing inflammatory bowel diseases in humans (Gentschew and Ferguson, 2012) and, providing the existence of a similar diet-microbiota-mucus axis, it may be possible to design improved probiotic and prebiotic options for treating conditions that involve defects in the colonic mucus layer.

Figure 5. Microbiota Transplant from Chow-Fed Mice Prevents Deterioration of the Colonic Mucus Layer upon WSD Feeding

For a Figure360 author presentation of Figure 5, see the figure legend at <https://doi.org/10.1016/j.chom.2017.11.004#mmc4>.

(A and B) Ten-week-old mice (n = 7–8 mice/group) were treated with an antibiotic cocktail (ABX: 1 g/L ampicillin, 1 g/L metronidazole, 0.5 g/L vancomycin, and 0.5 g/L neomycin) for 3 days and subsequently switched to a WSD (A). Mice received a weekly microbiota transplant either from WSD-fed donor mice (WSD → WSD) or from chow-fed donor mice (WSD → Chow). After 6 weeks metabolic parameters were determined (B).

(C) Confocal z stacks (left) calculated from the position of fluorescent 1- μ m beads (center) were used to determine penetrability of the inner colonic mucus layer (right). The median z stack is shown for each mouse. Turquoise, colonic tissue; red, bacteria-sized beads.

(D) Growth rate of the inner colonic mucus layer.

(E) Cecal fermentation products of WSD → WSD and WSD → Chow mice.

Data in (B)–(E) are presented as means \pm SEM. Statistical significance was determined by unpaired t test for normally distributed data and Mann-Whitney U test for not-normally distributed data with *p < 0.05 and **p < 0.01.

(F) Relative abundance of microbial taxa was determined by 16S rDNA analysis of colonic bacteria on phylum and genus level, for which abundances >1% are shown.

(G and H) α -Diversity (G) and β -diversity (weighted UniFrac) (H) for the colonic microbial community. Statistical significance for diversity analyses was calculated as described in the STAR Methods. See also Figure S3 and Table S1.

Figure360▶

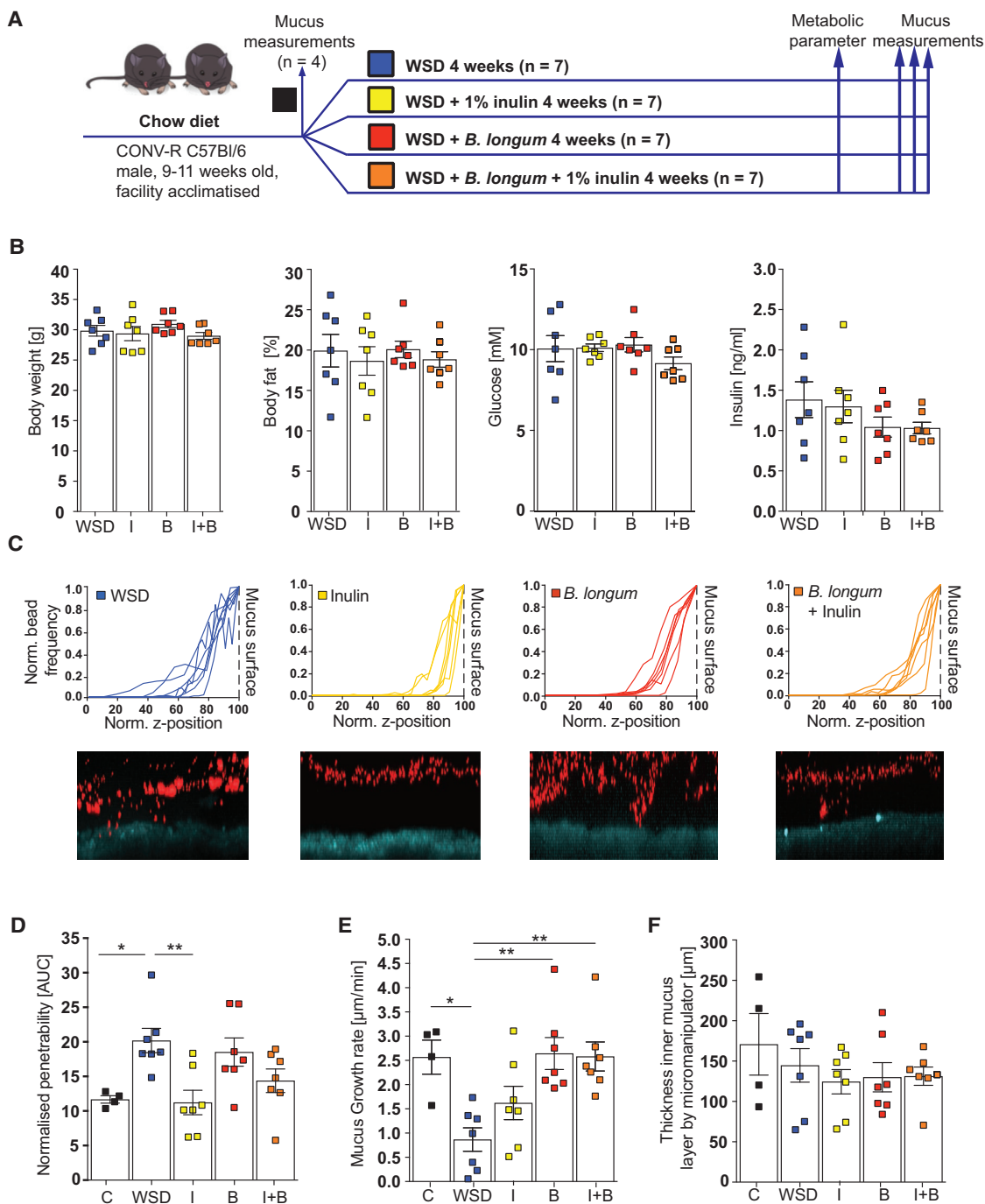


Figure 6. Probiotic and Prebiotic Supplements Prevent Distinct Aspects of Diet-Mediated Mucus Defects

(A) After mucus properties were analyzed in a control subset of mice (C) ($n = 4$), the remaining animals were divided into four groups ($n = 7$ per group) and switched to a WSD at the age of 9–11 weeks. Drinking water was supplemented with vehicle control (WSD), 1% (w/v) oligofructose-enriched inulin (I), *Bifidobacterium longum* NCC2705 (B), or a combination of both (B + I).

(B) Metabolic parameters were analyzed 3 weeks after the dietary switch and mucus measurements performed after 4 weeks on supplemented WSD.

(C) Confocal z stacks (top) calculated from the position of fluorescent 1- μm beads (bottom) were used to determine penetrability of the inner colonic mucus layer. The median z stack is shown for each mouse. Turquoise, colonic tissue; red, bacteria-sized beads.

(E and F) Growth rate (E) and thickness (F) of the inner colonic mucus layer. Data are presented as mean \pm SEM. Statistical significance against WSD-fed mice (vehicle control) was determined by Kruskal-Wallis test and corrected by Dunn's multiple comparisons test with * $p < 0.05$ and ** $p < 0.01$.

STAR★METHODS

Detailed methods are provided in the online version of this paper and include the following:

- KEY RESOURCES TABLE
- CONTACT FOR REAGENT AND RESOURCE SHARING
- EXPERIMENTAL MODEL AND SUBJECT DETAILS
 - Mice
 - Microbial Strains
- METHOD DETAILS
 - Metabolic Measurements
 - Explant *Ex Vivo* Mucus Thickness Measurements
 - Confocal Analysis of Mucus Layer Properties
 - Mucus Proteome Analyses
 - RNA Extraction from Colonic Tissue
 - Absolute Transcript Quantification by qPCR
 - Histology
 - Immunohistochemistry
 - Goblet Cell Count
 - DNA Extraction and 16S rRNA Gene Sequencing
 - Quantification of Fermentation Products
 - Western Style Diet Feeding for 0 - 28 Days
 - Caecal Microbiota Transplantation
 - *B. Longum* and Inulin Supplementation
- QUANTIFICATION AND STATISTICAL ANALYSIS
- DATA AND SOFTWARE AVAILABILITY

SUPPLEMENTAL INFORMATION

Supplemental Information includes three figures and two tables and can be found with this article online at <https://doi.org/10.1016/j.chom.2017.11.004>.

ACKNOWLEDGMENTS

We would like to thank Valentina Tremaroli and Rozita Akrami (University of Gothenburg) for bioinformatics assistance. Furthermore, we thank Zakarias Gulic and Caroline Wennberg for excellent animal husbandry, the Center for Cellular Imaging at the University of Gothenburg, Alsiano/Beneo for kindly providing inulin, and Nestlé for providing the *Bifidobacterium longum* NCC2705 strain. We thank Anna Hallén for assistance with the graphical abstract. The computations for microbiota composition analyses were performed on resources provided by the Swedish National Infrastructure for Computing (SNIC) through Uppsala Multidisciplinary Center for Advanced Computational Science (UPPMAX). Work in the authors' laboratories is supported by the Swedish Research Council, the NovoNordisk foundation, the Swedish Heart-Lung Foundation, Göran Gustafsson's Foundation, the IngaBritt och Arne Lundbergs Foundation, the Knut and Alice Wallenberg Foundation, the National Institute of Allergy and Infectious Diseases (U01AI095473), the content is solely the responsibility of the authors and does not necessarily represent the official views of the NIH), the Hasselblad foundation, the FP7 sponsored program METACARDIS, and the regional agreement on medical training and clinical research (ALF) between Region Västra Götaland and Sahlgrenska University Hospital. F.B. is Torsten Söderberg professor in medicine and recipient of a European Research Council Consolidator Grant (615362 – METABASE), G.C.H. is a recipient of a European Research Council Advanced Grant (694181 – MUC2GO), and B.O.S. is supported by a Marie Curie Intra European Fellowship (622909 – MUCUS AND METABOLISM) and a Human Frontier Science Program Long-Term Fellowship.

AUTHOR CONTRIBUTIONS

Conceptualization, B.O.S., G.M.H.B., G.C.H., and F.B.; Methodology, B.O.S., G.M.H.B., M.S., L.A., M.E.V.J., G.C.H., and F.B.; Investigation, B.O.S.,

G.M.H.B., M.S., and L.A.; Writing – Original Draft, B.O.S. and F.B.; Writing – Review & Editing, all authors; Funding Acquisition, G.C.H. and F.B.; Resources, G.C.H. and F.B.; Supervision, F.B.

Received: July 21, 2017

Revised: September 14, 2017

Accepted: October 20, 2017

Published: December 21, 2017

REFERENCES

- Ambort, D., Johansson, M.E.V., Gustafsson, J.K., Nilsson, H.E., Ermund, A., Johansson, B.R., Koeck, P.J.B., Hebert, H., and Hansson, G.C. (2012). Calcium and pH-dependent packing and release of the gel-forming MUC2 mucin. *Proc. Natl. Acad. Sci. USA* *109*, 5645–5650.
- Birchenough, G.M.H., Nyström, E.E.L., Johansson, M.E.V., and Hansson, G.C. (2016). A sentinel goblet cell guards the colonic crypt by triggering Nlrp6-dependent Muc2 secretion. *Science* *352*, 1535–1542.
- Bishara, J., Farah, R., Mograbi, J., Khalaila, W., Abu-Elheja, O., Mahamid, M., and Nseir, W. (2013). Obesity as a risk factor for *Clostridium difficile* infection. *Clin. Infect. Dis.* *57*, 489–493.
- Burcelin, R., Serino, M., Chabo, C., Garidou, L., Pomié, C., Courtney, M., Amar, J., and Bouloumié, A. (2013). Metagenome and metabolism: the tissue microbiota hypothesis. *Diabetes Obes. Metab.* *15*, 61–70.
- Caesar, R., Reigstad, C.S., Bäckhed, H.K., Reinhardt, C., Ketonen, M., Lundén, G.Ö., Cani, P.D., and Bäckhed, F. (2012). Gut-derived lipopolysaccharide augments adipose macrophage accumulation but is not essential for impaired glucose or insulin tolerance in mice. *Gut* *61*, 1701–1707.
- Cani, P.D., Amar, J., Iglesias, M.A., Poggi, M., Knauf, C., Bastelica, D., Neyrinck, A.M., Fava, F., Tuohy, K.M., Chabo, C., et al. (2007). Metabolic endotoxemia initiates obesity and insulin resistance. *Diabetes* *56*, 1761–1772.
- Caporaso, J.G., Kuczynski, J., Stombaugh, J., Bittinger, K., Bushman, F.D., Costello, E.K., Fierer, N., Peña, A.G., Goodrich, J.K., Gordon, J.I., et al. (2010a). QIIME allows analysis of high-throughput community sequencing data. *Nat. Methods* *7*, 335–336.
- Caporaso, J.G., Bittinger, K., Bushman, F.D., DeSantis, T.Z., Andersen, G.L., and Knight, R. (2010b). PyNAST: a flexible tool for aligning sequences to a template alignment. *Bioinformatics* *26*, 266–267.
- Chassaing, B., Raja, S.M., Lewis, J.D., Srinivasan, S., and Gewirtz, A.T. (2017). Colonic microbiota encroachment correlates with dysglycemia in humans. *Cell. Mol. Gastroenterol. Hepatol.* *4*, 205–221.
- Chung, H., Pamp, S.J., Hill, J.A., Surana, N.K., Edelman, S.M., Troy, E.B., Reading, N.C., Villablanca, E.J., Wang, S., Mora, J.R., et al. (2012). Gut immune maturation depends on colonization with a host-specific microbiota. *Cell* *149*, 1578–1593.
- Cotillard, A., Kennedy, S.P., Kong, L.C., Prifti, E., Pons, N., Le Chatelier, E., Almeida, M., Quinquis, B., Levenez, F., Galleron, N., et al. (2013). Dietary intervention impact on gut microbial gene richness. *Nature* *500*, 585–588.
- Cox, J., and Mann, M. (2008). MaxQuant enables high peptide identification rates, individualized p.p.b.-range mass accuracies and proteome-wide protein quantification. *Nat. Biotechnol.* *26*, 1367–1439.
- David, L.A., Maurice, C.F., Carmody, R.N., Gootenberg, D.B., Button, J.E., Wolfe, B.E., Ling, A.V., Devlin, A.S., Varma, Y., Fischbach, M.A., et al. (2014). Diet rapidly and reproducibly alters the human gut microbiome. *Nature* *505*, 559–563.
- Desai, M.S., Seekatz, A.M., Koropatkin, N.M., Kamada, N., Hickey, C.A., Wolter, M., Pudlo, N.A., Kitamoto, S., Terrapon, N., Muller, A., et al. (2016). A dietary fiber-deprived gut microbiota degrades the colonic mucus barrier and enhances pathogen susceptibility. *Cell* *167*, 1339–1353.e21.
- DeSantis, T.Z., Hugenholtz, P., Larsen, N., Rojas, M., Brodie, E.L., Keller, K., Huber, T., Dalevi, D., Hu, P., and Andersen, G.L. (2006). Greengenes, a chimera-checked 16S rRNA gene database and workbench compatible with ARB. *Appl. Environ. Microbiol.* *72*, 5069–5072.
- Dewulf, E.M., Cani, P.D., Neyrinck, A.M., Possemiers, S., Holle, A.V., Muccioli, G.G., Deldicque, L., Bindels, L.B., Pachikian, B.D., Sohet, F.M., et al. (2011).

- Inulin-type fructans with prebiotic properties counteract GPR43 overexpression and PPAR γ -related adipogenesis in the white adipose tissue of high-fat diet-fed mice. *J. Nutr. Biochem.* **22**, 712–722.
- Duranti, S., Gaiani, F., Mancabelli, L., Milani, C., Grandi, A., Bolchi, A., Santoni, A., Lugli, G.A., Ferrario, C., Mangifesta, M., et al. (2016). Elucidating the gut microbiome of ulcerative colitis: bifidobacteria as novel microbial biomarkers. *FEMS Microbiol. Ecol.* **92**, <https://doi.org/10.1093/femsec/fiw191>.
- Earle, K.A., Billings, G., Sigal, M., Lichtman, J.S., Hansson, G.C., Elias, J.E., Amieva, M.R., Huang, K.C., and Sonnenburg, J.L. (2015). Quantitative imaging of gut microbiota spatial organization. *Cell Host Microbe* **18**, 478–488.
- Edgar, R.C. (2010). Search and clustering orders of magnitude faster than BLAST. *Bioinformatics* **26**, 2460–2461.
- Everard, A., Lazarevic, V., Derrien, M., Girard, M., Muccioli, G.G., Neyrinck, A.M., Possemiers, S., Holle, A.V., François, P., de Vos, W.M., et al. (2011). Responses of gut microbiota and glucose and lipid metabolism to prebiotics in genetic obese and diet-induced leptin-resistant mice. *Diabetes* **60**, 2775–2786.
- Everard, A., Belzer, C., Geurts, L., Ouwerkerk, J.P., Druart, C., Bindels, L.B., Guiot, Y., Derrien, M., Muccioli, G.G., Delzenne, N.M., et al. (2013). Cross-talk between *Akkermansia muciniphila* and intestinal epithelium controls diet-induced obesity. *Proc. Natl. Acad. Sci. USA* **110**, 9066–9071.
- Faith, D.P. (1992). Conservation evaluation and phylogenetic diversity. *Biol. Conserv.* **61**, 1–10.
- Filippo, C.D., Cavalleri, D., Paola, M.D., Ramazzotti, M., Pouillet, J.B., Massart, S., Collini, S., Pieraccini, G., and Lionetti, P. (2010). Impact of diet in shaping gut microbiota revealed by a comparative study in children from Europe and rural Africa. *Proc. Natl. Acad. Sci. USA* **107**, 14691–14696.
- Fu, J., Wei, B., Wen, T., Johansson, M., Liu, X., Bradford, E., Thomsson, K., McGee, S., Mansour, L., Tong, M., et al. (2011). Loss of intestinal core 1-derived O-glycans causes spontaneous colitis in mice. *J. Clin. Invest.* **121**, 1657–1723.
- Fukuda, S., Toh, H., Hase, K., Oshima, K., Nakanishi, Y., Yoshimura, K., Tobe, T., Clarke, J., Topping, D., Suzuki, T., et al. (2011). Bifidobacteria can protect from enteropathogenic infection through production of acetate. *Nature* **469**, 543–550.
- Gentschew, L., and Ferguson, L.R. (2012). Role of nutrition and microbiota in susceptibility to inflammatory bowel diseases. *Mol. Nutr. Food Res.* **56**, 524–535.
- Gibson, G.R., Beatty, E.R., Wang, X., and Cummings, J.H. (1995). Selective stimulation of bifidobacteria in the human colon by oligofructose and inulin. *Gastroenterology* **108**, 975–982.
- Gustafsson, J.K., Ermund, A., Johansson, M.E.V., Schütte, A., Hansson, G.C., and Sjövall, H. (2012). An ex vivo method for studying mucus formation, properties, and thickness in human colonic biopsies and mouse small and large intestinal explants. *Am. J. Physiol. Gastrointest. Liver Physiol.* **302**, G430–G438.
- Haas, B.J., Gevers, D., Earl, A.M., Feldgarden, M., Ward, D.V., Giannoukos, G., Ciulla, D., Tabbaa, D., Highlander, S.K., Sodergren, E., et al. (2011). Chimeric 16S rRNA sequence formation and detection in Sanger and 454-pyrosequenced PCR amplicons. *Genome Res.* **21**, 494–504.
- Hansson, G.C., Baekstrom, D., Carlstedt, I., and Klinga-Levan, K. (1994). Molecular cloning of a cDNA coding for a region of an apoprotein from the insoluble mucin complex of rat small intestine. *Biochem. Biophys. Res. Commun.* **198**, 181–190.
- He, F., Ouwehand, A.C., Hashimoto, H., Isolauri, E., Benno, Y., and Salminen, S. (2001). Adhesion of bifidobacterium spp. to human intestinal mucus. *Microbiol. Immunol.* **45**, 259–262.
- Heazlewood, C.K., Cook, M.C., Eri, R., Price, G.R., Tauro, S.B., Taupin, D., Thornton, D.J., Png, C.W., Crockford, T.L., Cornall, R.J., et al. (2008). Aberrant mucin assembly in mice causes endoplasmic reticulum stress and spontaneous inflammation resembling ulcerative colitis. *PLoS Med.* **5**, e54.
- Hildebrandt, M.A., Hoffmann, C., Sherrill-Mix, S.A., Keilbaugh, S.A., Hamady, M., Chen, Y., Knight, R., Ahima, R.S., Bushman, F., and Wu, G.D. (2009). High-fat diet determines the composition of the murine gut microbiome independently of obesity. *Gastroenterology* **137**, 1716–1724.e1–2.
- Jakobsson, H.E., Rodríguez-Piñeiro, A.M., Schütte, A., Ermund, A., Boysen, P., Bemark, M., Sommer, F., Bäckhed, F., Hansson, G.C., and Johansson, M.E. (2015). The composition of the gut microbiota shapes the colon mucus barrier. *EMBO Rep.* **16**, 164–177.
- Johansson, M.E.V. (2012). Fast renewal of the distal colonic mucus layers by the surface goblet cells as measured by in vivo labeling of mucin glycoproteins. *PLoS One* **7**, e41009.
- Johansson, M.E.V., Phillipson, M., Petersson, J., Velcich, A., Holm, L., and Hansson, G.C. (2008). The inner of the two Muc2 mucin-dependent mucus layers in colon is devoid of bacteria. *Proc. Natl. Acad. Sci. USA* **105**, 15064–15069.
- Johansson, M.E.V., Gustafsson, J.K., Holmén-Larsson, J., Jabbar, K.S., Xia, L., Xu, H., Ghishan, F.K., Carvalho, F.A., Gewirtz, A.T., Sjövall, H., et al. (2014). Bacteria penetrate the normally impenetrable inner colon mucus layer in both murine colitis models and patients with ulcerative colitis. *Gut* **63**, 281–291.
- Kaoutari, A.E., Armougoum, F., Gordon, J.I., Raoult, D., and Henrissat, B. (2013). The abundance and variety of carbohydrate-active enzymes in the human gut microbiota. *Nat. Rev. Microbiol.* **11**, 497–504.
- Koh, A., De Vadder, F., Kovatcheva-Datchary, P., and Bäckhed, F. (2016). From dietary fiber to host physiology: short-chain fatty acids as key bacterial metabolites. *Cell* **165**, 1332–1345.
- Kozich, J.J., Westcott, S.L., Baxter, N.T., Highlander, S.K., and Schloss, P.D. (2013). Development of a dual-index sequencing strategy and curation pipeline for analyzing amplicon sequence data on the MiSeq Illumina sequencing platform. *Appl. Environ. Microbiol.* **79**, 5112–5120.
- Kumar, S.A., Ward, L.C., and Brown, L. (2016). Inulin oligofructose attenuates metabolic syndrome in high-carbohydrate, high-fat diet-fed rats. *Br. J. Nutr.* **116**, 1502–1511.
- Madsen, J., Mollenhauer, J., and Holmskov, U. (2010). Review: Gp-340/DMBT1 in mucosal innate immunity. *Innate Immun.* **16**, 160–167.
- Martens, E.C., Chiang, H.C., and Gordon, J.I. (2008). Mucosal glycan foraging enhances fitness and transmission of a saccharolytic human gut bacterial symbiont. *Cell Host Microbe* **4**, 447–457.
- Ormerod, K.L., Wood, D.L.A., Lachner, N., Gellatly, S.L., Daly, J.N., Parsons, J.D., Dal'Molin, C.G.O., Palfreyman, R.W., Nielsen, L.K., Cooper, M.A., et al. (2016). Genomic characterization of the uncultured Bacteroidales family S24-7 inhabiting the guts of homeothermic animals. *Microbiome* **4**, 36.
- Picard, C., Fioramonti, J., Francois, A., Robinson, T., Neant, F., and Matuchansky, C. (2005). Review article: bifidobacteria as probiotic agents – physiological effects and clinical benefits. *Aliment. Pharmacol. Ther.* **22**, 495–512.
- Price, M.N., Dehal, P.S., and Arkin, A.P. (2010). FastTree 2 – approximately maximum-likelihood trees for large alignments. *PLoS One* **5**, e9490.
- Rappsilber, J., Mann, M., and Ishihama, Y. (2007). Protocol for micro-purification, enrichment, pre-fractionation and storage of peptides for proteomics using stagetips. *Nat. Protoc.* **2**, 1896–1906.
- Rossi, M., Corradini, C., Amaretti, A., Nicolini, M., Pompei, A., Zanoni, S., and Matteuzzi, D. (2005). Fermentation of fructooligosaccharides and inulin by bifidobacteria: a comparative study of pure and fecal cultures. *Appl. Environ. Microbiol.* **71**, 6150–6158.
- Salonen, A., Nikkilä, J., Jalanka-Tuovinen, J., Immonen, O., Rajilic-Stojanovic, M., Kekkonen, R.A., Palva, A., and de Vos, W.M. (2010). Comparative analysis of fecal DNA extraction methods with phylogenetic microarray: effective recovery of bacterial and archaeal DNA using mechanical cell lysis. *J. Microbiol. Methods* **81**, 127–134.
- Schnorr, S.L., Candela, M., Rampelli, S., Centanni, M., Consolandi, C., Basaglia, G., Turrioni, S., Biagi, E., Peano, C., Severgnini, M., et al. (2014). Gut microbiome of the Hadza hunter-gatherers. *Nat. Commun.* **5**, 3654.
- Schroeder, B.O., and Bäckhed, F. (2016). Signals from the gut microbiota to distant organs in physiology and disease. *Nat. Med.* **22**, 1079–1089.

- Sonnenburg, E.D., Smits, S.A., Tikhonov, M., Higginbottom, S.K., Wingreen, N.S., and Sonnenburg, J.L. (2016). Diet-induced extinctions in the gut microbiota compound over generations. *Nature* 529, 212–215.
- Sonnenburg, J.L., Xu, J., Leip, D.D., Chen, C.-H., Westover, B.P., Weatherford, J., Buhler, J.D., and Gordon, J.I. (2005). Glycan foraging in vivo by an intestine-adapted bacterial symbiont. *Science* 307, 1955–1959.
- Teixeira, T.F.S., Souza, N.C.S., Chiarello, P.G., Franceschini, S.C.C., Bressan, J., Ferreira, C.L.L.F., and Peluzio Mdo, C.G. (2012). Intestinal permeability parameters in obese patients are correlated with metabolic syndrome risk factors. *Clin. Nutr.* 31, 735–740.
- Turnbaugh, P.J., Bäckhed, F., Fulton, L., and Gordon, J.I. (2008). Diet-induced obesity is linked to marked but reversible alterations in the mouse distal gut microbiome. *Cell Host Microbe* 3, 213–223.
- Turnbaugh, P.J., Ridaura, V.K., Faith, J.J., Rey, F.E., Knight, R., and Gordon, J.I. (2009). The effect of diet on the human gut microbiome: a metagenomic analysis in humanized gnotobiotic mice. *Sci. Transl. Med.* 1, 6ra14.
- Tyanova, S., Temu, T., Sinitcyn, P., Carlson, A., Hein, M.Y., Geiger, T., Mann, M., and Cox, J. (2016). The Perseus computational platform for comprehensive analysis of (prote)omics data. *Nat. Methods* 13, 731–740.
- Vandeputte, D., Falony, G., Vieira-Silva, S., Wang, J., Sailer, M., Theis, S., Verbeke, K., and Raes, J. (2017). Prebiotic inulin-type fructans induce specific changes in the human gut microbiota. *Gut* 66, 1968–1974.
- Vizcaino, J.A., Csordas, A., del-Toro, N., Dianes, J.A., Griss, J., Lavidas, I., Mayer, G., Perez-Riverol, Y., Reisinger, F., Ternent, T., et al. (2016). 2016 update of the PRIDE database and its related tools. *Nucleic Acids Res.* 44, D447–D456.
- Wang, Q., Garrity, G.M., Tiedje, J.M., and Cole, J.R. (2007). Naïve Bayesian classifier for rapid assignment of rRNA sequences into the new bacterial taxonomy. *Appl. Environ. Microbiol.* 73, 5261–5267.
- Wichmann, A., Allahyar, A., Greiner, T.U., Plovier, H., Lundén, G.Ö., Larsson, T., Drucker, D.J., Delzenne, N.M., Cani, P.D., and Bäckhed, F. (2013). Microbial modulation of energy availability in the colon regulates intestinal transit. *Cell Host Microbe* 14, 582–590.
- Wiśniewski, J.R., Zougman, A., Nagaraj, N., and Mann, M. (2009). Universal sample preparation method for proteome analysis. *Nat. Methods* 6, 359–362.
- Yatsunenko, T., Rey, F.E., Manary, M.J., Trehan, I., Dominguez-Bello, M.G., Contreras, M., Magris, M., Hidalgo, G., Baldassano, R.N., Anokhin, A.P., et al. (2012). Human gut microbiome viewed across age and geography. *Nature* 486, 222–227.
- Zhang, J., Kobert, K., Flouri, T., and Stamatakis, A. (2014). PEAR: a fast and accurate illumina paired-end reAd mergeR. *Bioinformatics* 30, 614–620.

STAR★METHODS

KEY RESOURCES TABLE

REAGENT or RESOURCE	SOURCE	IDENTIFIER
Antibodies		
Rabbit polyclonal anti-Muc2 (Muc2C3)	Johansson et al., 2008	N/A
Rabbit polyclonal anti-apo-Muc2 (PH497)	Hansson et al., 1994	N/A
Bacterial and Virus Strains		
Bifidobacterium longum NCC2705	Nestlé	N/A
Chemicals, Peptides, and Recombinant Proteins		
GuHCl 8M	Thermo Scientific	24115
DTT	Sigma-Aldrich	D9163
Iodoacetamide	Sigma-Aldrich	I6125
LysC	Wako	125-05061
Trypsin	Promega	V5111
Mouse Muc2 SpikeTides_L Proteotypic Peptides	JPT	N/A
Fat adjusted diet	Envigo	TD.96132
Autoclavable Mouse Breeder Diet	LabDiet	5021
Isoflurane	Kronans apotek	N01AB06
2X cOmplete Protease Inhibitor Cocktail	Roche	11873580001
Lysing matrix E	MPBio	116914100
Sodium isovalerate-1- ¹³ C	Sigma-Aldrich	487643
Isobutyric acid-1- ¹³ C	Sigma-Aldrich	606138
Sodium butyrate- ¹³ C ₄	Sigma-Aldrich	488380
Propionic acid-d ₆	Sigma-Aldrich	490644
Sodium acetate-1- ¹³ C,d ₃	Sigma-Aldrich	298042
Succinic acid ¹³ C ₄	Cambride Isotope Laboratories	CLM-1571
Sodium lactate ¹³ C ₃	Cambride Isotope Laboratories	CLM-1579
N-tert-butylidimethylsilyl-N-methyltrifluoroacetamide	Sigma-Aldrich	394882
Ampicillin	Sigma-Aldrich	A9518-100G
Metronidazole	Sigma-Aldrich	M3761-5G
Vancomycin	Sigma-Aldrich	V2002-5G
Neomycin	Sigma-Aldrich	N6386-100G
Black 10μm polystyrene Polybead microspheres	Polysciences	24294
Crimson 1μm Fluospheres	Thermo Fisher Scientific	F8816
Calcein violet AM	Thermo Fisher Scientific	C34858
Hoechst-34580	Sigma-Aldrich	63493
Oligofructose-enriched inulin (Orafti Synergy 1)	Alsiano/Beneo	http://www.beneo.com
Difco Reinforced Clostridial Medium	BD	218081
Critical Commercial Assays		
Bayer Contour Next blood glucose strips	Kronans apotek	732781
Ultra Sensitive Mouse Insulin ELISA kit	Crystal Chem	90080
RNeasy Mini kit	Qiagen	74106
High Capacity cDNA Reverse Transcription Kit	Thermo Fisher Scientific	4368814
HotStarTaq Master mix Kit	Qiagen	203445
pGEM-T Vector Systems	Promega	A3600
One Shot MAX Efficiency DH10B T1 cells	Invitrogen	12331-013
QIAprep Spin Miniprep Kit	Qiagen	27106

(Continued on next page)

Continued

REAGENT or RESOURCE	SOURCE	IDENTIFIER
1x SYBR Green Master Mix	Thermo Fisher Scientific	4309155
5PRIME HotMasterMix	Quantabio	733-2474
NucleoSpin Gel and PCR Clean-up kit	Macherey-Nagel	740609
Quant-iT PicoGreen dsDNA Assay kit	Thermo Fisher Scientific	P11496
Agencourt AMPure XP	Beckman Coulter	A63880
Deposited Data		
Proteomics data raw data	This paper	ProteomeXchange: PXD006129
Microbiota 16S rDNA gene sequences	This paper	ENA: PRJEB20367
Greengenes reference database	DeSantis et al., 2006	http://greengenes.lbl.gov
Experimental Models: Organisms/Strains		
Male C57BL/6J mice	Charles River Germany	000664 Black 6
Male heterozygous Ob/WT mice B6.Cg-Lepob/J	Charles River Italy	000632 B6 ob
Female heterozygous Ob/WT mice B6.Cg-Lepob/J	Charles River Italy	000632 B6 ob
Male C57BL/6J mice	own breeding	N/A
Oligonucleotides		
V4 region 515F and 806R primers	Kozich et al., 2013	N/A
Dmbt1 F 5'-GGGGATCTCCACTGTTATCTTTGA-3'	Sigma-Aldrich	N/A
Dmbt1 R 5'-AGAATCTGTTCCATCTGTGGGA-3'	Sigma-Aldrich	N/A
Recombinant DNA		
pGEM-T-Dmbt1	This paper	N/A
Software and Algorithms		
MaxQuant	Cox and Mann, 2008	http://www.biochem.mpg.de/5111795/maxquant
Perseus	Tyanova et al., 2016	http://www.biochem.mpg.de/5111810/perseus
Prism (version 7.0b)	GraphPad	https://www.graphpad.com/scientific-software/prism/
QIIME (version 1.9.1).	Caporaso et al., 2010a	http://qiime.org
Mouse mucin sequence database	in-house database	http://www.medkem.gu.se/mucinbiology/databases/
PEAR	Zhang et al., 2014	http://www.exelixis-lab.org/web/software/pear
UCLUST	Edgar, 2010	http://www.drive5.com/usearch/
Imaris (version 7.6.3)	Bitplane	http://www.bitplane.com
Zen (version 2.3)	Carl Zeiss	http://www.zeiss.com
PyNAST	Caporaso et al., 2010b	http://pynast.sourceforge.net
FastTree	Price et al., 2010	http://www.microbesonline.org/fasttree
ChimeraSlayer	Haas et al., 2011	http://microbiomeutil.sourceforge.net/#A_CS
Other		
Nanosep 10K Omega	Pall, Life Sciences	OD010C35
EchoMRI Body Composition Analyzers for Live Small Animals	Echo Medical Systems	http://www.echomri.com
EASY-nLC system 1000	Thermo Scientific	LC120
reverse-phase column (150 × 0.075 mm inner diameter, C18-AQ 3 μm)	in-house packed	N/A
QExactive Hybrid Quadrupole-Orbitrap Mass Spectrometer	Thermo Scientific	IQLAAEGAAPFALGMAZR
StageTip C18 columns	Rappsilber et al., 2007	N/A
TissueLyser II	Qiagen	85300
QiaCube	Qiagen	9001885
NanoDrop ND-1000 spectrophotometer	Thermo Scientific	http://www.nanodrop.com/Products.aspx
CFX96 Real-Time PCR Detection System	Bio-Rad	C1000

(Continued on next page)

Continued

REAGENT or RESOURCE	SOURCE	IDENTIFIER
Illumina MiSeq	Illumina	https://www.illumina.com/systems/sequencing-platforms/miseq.html
Fast-Prep-24 Classic	MPBio	116004500
Gas Chromatograph-Mass Spectrometer	Agilent Technologies	7890A + 5975C series
Anaerobic COY chamber	COY Laboratory Products	http://coylab.com/products/anaerobic-chambers/vinyl-anaerobic-chambers/
Horizontal perfusion chamber	Gustafsson et al., 2012	N/A
Perfusion chamber heating blocks	Gustafsson et al., 2012	N/A
Dual automatic temperature controller	Warner instruments	TC-344B
DDS syringe pump	Harvard apparatus	70-3333
LED light source	Photonic optics	F3000
Stereo-microscope	Lecia	MZ75
Digimatic micrometer	Mitutoyo	350-261-30
Digimatic interface	Mitutoyo	264-014-10
Borosilicate glass capillaries	Sutter instrument	BF120-60-10
Flaming/Brown Micropipette Puller	Sutter instrument	P-97
Laser scanning confocal imaging system	Carl Zeiss	LSM700

CONTACT FOR REAGENT AND RESOURCE SHARING

Further information and requests for resources and reagents should be directed to and will be fulfilled by the Lead Contact, Fredrik Bäckhed (fredrik.backhed@wlab.gu.se).

EXPERIMENTAL MODEL AND SUBJECT DETAILS**Mice**

Male wild-type C57BL/6J mice were co-housed with 5 mice/cage under specific pathogen free (SPF) conditions at a 12 hour light/dark cycle, had unlimited access to water and food and were either bred in-house or, when obtained from Charles River, Germany, acclimated to the facility for three weeks in cages with bedding that has previously been exposed to facility-resident mice. Leptin deficient Ob/Ob^{-/-} mice on a C57BL/6J background were originally obtained as heterozygous pairs from Charles River, Italy, bred in-house and co-housed with their lean littermates. 6 obese male and female Ob/Ob mice are compared against 6 lean (1 heterozygous Ob/Wt and 5 Wt/Wt) mice. For details see the following table. All mice used were age matched (15-17 weeks old; 13-15 weeks for *Bifidobacterium longum*/inulin treatment) and fed a standard chow diet (5021 LabDiet: 4.62 kcal/g; 23.7% kcal from fat (31% saturated, 33% mono-unsaturated, 36% polyunsaturated fatty acid), 53.2% from carbohydrates (sucrose 0.71% (w/v), starch 31.0% (w/v) glucose 0.21% (w/v), neutral detergent fiber 15.2% (w/v)) or a Western style diet (TD.96132 Envigo: 4.5 kcal/g; 40.6% kcal from fat (41% saturated, 52% mono-unsaturated, 7% polyunsaturated fatty acids), 40.7% from carbohydrates (sucrose 18.2% (w/v), corn starch 16.0% (w/v), maltodextrin 12.0% (w/v), cellulose 4.0% (w/v)). Animals were anesthetized using isoflurane and killed by cervical dislocation prior to sample collection. Sampling time during the day was matched between dietary/genetic groups and all experiments were performed using protocols approved by the University of Gothenburg Animal Studies Committee.

Source, Housing Conditions, and Experimental Setup of Mice

	Figures	Breeding	Facility Acclimatization	Littermates	Male	Female	Western Diet
Mucus measurements WSD	1, 2, and 3	in-house		X	X		8 weeks
Mucus measurements Ob/Ob	S1	in-house		X	X	X	–
Microbiota analyses WSD	3	Charles River	X		X		8 weeks
Mucus phenotype time course	2 and 4	Charles River	X		X		1–28 days
Mucus phenotype prevention	2, 5, and S2	Charles River	X		X		6 weeks
Bifidobacterium/inulin treatment	6	Charles River	X		X		4 weeks

Microbial Strains

Bifidobacterium (B.) longum NCC2705 was kindly provided by Nestec, Nestlé Research Center (Lausanne, Switzerland). Culture was maintained on Reinforced Clostridial Medium (RCM, BD Difco, CA) agar plates in a Coy Anaerobic Chamber (Coy, MI) with a gas mix containing 5% hydrogen, 10% carbon dioxide and 85% nitrogen. Purity of the culture was monitored by Gram-staining and plating of serial dilutions.

B. longum culture was inoculated into fresh liquid RCM and incubated anaerobically for 24 hours, mixed with autoclaved glycerol (20% final) and stored at -80°C (about 2×10^8 colony forming units/ ml) until further usage.

METHOD DETAILS

Metabolic Measurements

Mice were fasted for 4 hours and glucose concentration was measured in tail vein whole blood with commercial blood glucose strips (Contour Next, Bayer, Germany). Insulin concentration was determined in serum by Ultra Sensitive Mouse Insulin ELISA kit (Crystal Chem, IL). Body fat was determined by whole-body magnetic resonance imaging (EchoMRI, Echo Medical Systems, TX).

Explant Ex Vivo Mucus Thickness Measurements

Thickness of the inner mucus layer was measured on alive tissue as described (Birchenough et al., 2016; Gustafsson et al., 2012). Briefly, intestinal tissue was flushed with cold Krebs buffer to remove luminal content and unattached mucus (“outer layer”). The muscle layer was removed by microdissection and the distal colon was mounted in a horizontal chamber system and maintained at 37°C with basolateral Krebs-glucose buffer perfusion and apical Krebs-mannitol buffer. For visualization of the mucus surface black $10\ \mu\text{m}$ polystyrene Polybead microspheres (Polysciences, Germany) were added apically. The surface was observed by a stereomicroscope and mucus thickness measured using a glass micropipette connected to a micrometer. Mucus thickness was measured every 15 min at five different locations for up to 45 minutes.

Confocal Analysis of Mucus Layer Properties

Colonic inner mucus layer barrier function was assessed by quantifying penetrability to $1\ \mu\text{m}$ bacteria sized microbeads by use of confocal microscopy. Flushed distal colonic tissue was prepared and mounted in a horizontal perfusion chamber as previously described (Gustafsson et al., 2012). The tissue was stained by adding Calcein violet AM (Thermo Fisher Scientific, MA; $1\ \mu\text{g}/\text{ml}$) to the basolateral Krebs-glucose buffer and the apical mucosal surface was overlaid with $1\ \mu\text{m}$ diameter Fluosphere crimson microbeads (Thermo Fisher, 1:10) diluted in $10\ \mu\text{l}$ Krebs-mannitol buffer. Microbeads were allowed to sediment onto the mucus surface for 5 min and the mucosal surface was gently washed with $0.5\ \text{ml}$ Krebs-mannitol to remove excess microbeads. The apical perfusion chamber compartment was then filled with $2\ \text{ml}$ Krebs mannitol and the perfusion chamber was transferred to an LSM700 confocal imaging system (Carl Zeiss, Germany). Tissue and microbeads were visualized by acquiring confocal z-stacks using a x20 water immersion objective lens, 405/639 nm lasers and Zen acquisition software (Carl Zeiss). Zen files were imported into Imaris software (Bitplane) and isosurfaces were mapped to Calcein violet (tissue) and Fluosphere (microbeads) fluorescent signals. Data describing the z-axis position of the tissue and individual microbeads was extracted and the mucus layer thickness was quantified by calculating the average tissue-microbead z-axis distance. Mucus penetrability was quantified by analysis of microbead distribution within the mucus layer. Initially, a frequency distribution curve of tissue-microbead z-axis distance data was generated for each z-stack using Prism 6 software (Graphpad). To allow comparison of distribution curves acquired from different z-stacks, curves were first normalized to maximum frequency values in order to correct for differences in the absolute number of microbeads detected in each z-stack. Subsequently curves were normalized to the position of the mucus surface (the z-axis position with the maximum microbead frequency) in order to correct for variable mucus layer thickness, and were cropped to exclude data from microbeads above the mucus surface. Area under the curve (AUC) data was generated for each normalized distribution curve and expressed as ‘normalised penetrability’ in order to allow quantitative comparison of microbead penetration into the mucus layers of different samples.

Mucus Proteome Analyses

After *ex vivo* mucus measurements mucus was collected, 2X cOmplete Protease Inhibitor Cocktail (Merck) was added and samples were stored at -80°C until further processing. For proteome analyses isolated mucus samples were incubated overnight at 37°C in reduction buffer (6M guanidinium hydrochloride (GuHCl), 0.1M Tris/HCl, pH 8.5 (Merck), 5mM EDTA, 0.1 MDTT (Merck)) and all liquid added on top of a spin-filter (10 kDa, PALL, Port Washington, NY) for a filter-aided sample preparation following a previous protocol (Wiśniewski et al., 2009) where 6M GuHCl was used instead of urea. Proteins were alkylated on 10 kDa cut-off filters and subsequently digested for 4h with LysC (Wako, Richmond, VA) followed by an overnight trypsin (Promega, Fitchburg, WI) digestion. Heavy peptides (SpikeTides TQL, JPT Peptide Technologies, Berlin, Germany) for Muc2 absolute quantification (10 peptides, 100 fmol each; Table S2) were added before trypsin digestion.

Peptides released from the filter after centrifugation were cleaned with StageTip C18 columns (Rappsilber et al., 2007). NanoLC-MS/MS was performed on an EASY-nLC 1000 system (Thermo Fisher Scientific, Odense, Denmark), connected to a QExactive Hybrid Quadrupole-Orbitrap Mass Spectrometer (Thermo Fisher Scientific) through a nanoelectrospray ion source. Peptides were separated with an in-house packed reverse-phase column ($150 \times 0.075\ \text{mm}$ inner diameter, C18-AQ $3\ \mu\text{m}$) by a

60-min gradient from 5 to 40% of buffer B (A: 0.1% formic acid, B: 0.1% formic acid/ 80% acetonitrile) using a flow rate of 200 nl/min. Full mass spectra were acquired from 320–1,600 m/z with resolution of 70,000 (m/z 200). Up to twelve most intense peaks (charge state ≥ 2) were fragmented and tandem mass spectrum was acquired with a resolution of 35,000 and automatic dynamic exclusion. For absolute quantification a separate targeted mass spectrometry method was used where only precursors and their fragments of the heavy and corresponding light peptides were scanned with a resolution of 35,000.

Proteins were identified with the MaxQuant program (version 1.5.7.4; [Cox and Mann, 2008](#)) by searching against the mouse UniProt protein database (downloaded 23.07.2015) supplemented with an in-house database containing all the mouse mucin sequences (<http://www.medkem.gu.se/mucinbiology/databases/>). Searches were performed with full tryptic specificity, maximum 2 missed cleavages, precursor tolerance of 20 ppm in the first search used for recalibration, followed by 7 ppm for the main search and 0.5 Da for fragment ions. Carbamidomethylation of cysteine was set as a fixed modification and methionine oxidation and protein N-terminal acetylation were set as variable modification. The required false discovery rate (FDR) was set to 1% both for peptide and protein levels and the minimum required peptide length was set to six amino acids. Proteins were quantified based on MaxQuant label-free quantification (LFQ) option using a minimum of two peptides for quantification. Data filtering, clustering and principal component analysis (PCA) was performed with Perseus software (version 1.4.1.3). The data was filtered based on the presence of a protein group in at least three out of five biological replicates. Missing values were replaced from normal distribution using default values ([Tyanova et al., 2016](#)). Clustering and heatmap were performed using Euclidean distance, average linkage, preprocessing with k-means for rows and columns. For principal component analysis default parameters were used ([Tyanova et al., 2016](#)).

The mass spectrometry proteomics data were deposited to the ProteomeXchange Consortium (<http://proteomecentral.proteomexchange.org>) via the PRIDE partner repository ([Vizcaino et al., 2016](#)) with the dataset identifier ProteomeXchange: PXD006129.

RNA Extraction from Colonic Tissue

Intestinal mouse tissue was homogenized by using a TissueLyser II (Qiagen, Germany) and RNA was extracted with RNeasy Mini kit (Qiagen) using the Qiacube system (Qiagen) following the manufactures protocol. RNA quantity and quality were examined with a NanoDrop ND-1000 spectrophotometer (NanoDrop Technologies, Thermo Fisher Scientific). 500 ng of total RNA were transcribed into cDNA (High Capacity cDNA Reverse Transcription Kit, Thermo Fisher Scientific) and diluted 1:6 in dH₂O.

Absolute Transcript Quantification by qPCR

Mouse cDNA was amplified with gene-specific primers (Sigma; [Key Resources Table](#)) and HotStarTaq Master Mix Kit (Qiagen). Amplicons were cloned into pGEM-T vector (Promega, WI) and transformed into One Shot MAX Efficiency DH10B T1 cells (Invitrogen, CA). Plasmids were isolated (Qiagen Plasmid Mini Kit), sequenced (eurofins Genomics, Ebersberg, Germany), quantified and diluted in series of 10. Mouse samples were analyzed in a 12.5- μ l reaction mix consisting of 1x SYBR Green Master Mix buffer (Thermo Fisher Scientific), 0.2 μ M of custom-made primers (Sigma; [Key Resources Table](#)) and 2.5 μ l of template cDNA on a CFX96 Real-Time System (Bio-Rad). Transcript copy numbers were quantified by standard curves derived from the 10-fold plasmid dilutions described above.

Histology

Fresh intestinal mouse tissue was fixed in water-free Methacarn solution (Carnoy, 60% dry methanol, 30% chloroform, 10% glacial acetic acid) for at least 24 hours and processed into paraffin-embedded tissue sections by the Skandinaviskt Centrum för Histoteknik in Gothenburg, Sweden. One section per samples was stained with Alcian-Blue/ Periodic acid–Schiff (AB/PAS) to evaluate polysaccharide structures.

Immunohistochemistry

Paraffin-embedded tissue slides were de-waxed and antigen retrieval was carried out in 10 mM citrate buffer, pH 6.0. Tissue was blocked in 5% fetal calf serum (FCS), washed in PBS and incubated with primary antibodies (α Muc2(mature): Rabbit Muc2-C3, α Muc2(non-O-glycosylated): Rabbit Muc2-PH497), diluted in FCS over night. After another washing step tissue sections were incubated with a fluorophore-conjugated secondary antibody (Donkey α -Rabbit AF 488, Thermo Fisher Scientific) diluted in block solution for 2 hours. DNA was stained with Hoechst-34580 (Sigma-Aldrich; 5 μ g/ml) in PBS for 5 min, slides were washed in dH₂O, dried and mounted in a small volume of Prolong-Gold Antifade mounting medium (Thermo Fisher Scientific).

Goblet Cell Count

Goblet cell number was independently investigated in Carnoy-fixed colonic tissue sections by two blinded scientists. Only crypts that were cut longitudinally from crypt opening to bottom of the crypt were considered.

DNA Extraction and 16S rRNA Gene Sequencing

Genomic DNA from mucosal tissue, content and feces was extracted by repeated bead-beating using a Fast-Prep System with Lysing Matrix E (MPBio, CA) as described previously ([Salonen et al., 2010](#)). Bacterial DNA present in luminal content and intestinal tissue was profiled by sequencing of the V4 region of the 16S rRNA gene on an Illumina MiSeq (Illumina RTA v1.17.28; MCS v2.5) using 515F and 806R primers designed for dual indexing ([Kozich et al., 2013](#)) and the V2 kit (2x250 bp paired-end reads). Intestinal content

samples were amplified in duplicates whereas mucosa-associated bacteria (MAB) samples were amplified in triplicates in reaction volumes of 25 μ l containing 1x Five Prime Hot Master Mix (Quantabio, MA), 200 nM of each primer, 0.4 mg/ml BSA, 5% DMSO and 20 ng (content samples) or 100 ng (MAB) of genomic DNA. PCR was carried out under the following conditions: initial denaturation for 3 min at 94°C, followed by 25 cycles (content samples) or 28 cycles (MAB samples) of denaturation for 45 sec at 94°C, annealing for 60 sec at 52°C and elongation for 90 sec at 72°C, and a final elongation step for 10 min at 72°C. Replicates were combined, purified with the NucleoSpin Gel and PCR Clean-up kit (Macherey-Nagel, Germany) and quantified using the Quant-iT PicoGreen dsDNA kit (Thermo Fisher Scientific). Equal amounts of purified PCR products were pooled and the pooled PCR products were purified again using Ampure magnetic purification beads (Agencourt, Danvers, MA) to remove short amplification products.

Illumina paired-end reads were merged using PEAR (Zhang et al., 2014), and quality filtered to remove reads that had at least one base with a q-score lower than 20 and that were shorter than 220 nucleotides or longer than 350 nucleotides. Quality filtered reads were analyzed with the software package QIIME (Caporaso et al., 2010a) (version 1.9.1). Sequences were clustered into operational taxonomic units (OTUs) at a 97% identity threshold using an open-reference OTU picking approach with UCLUST (Edgar, 2010) against the Greengenes reference database (DeSantis et al., 2006) (13_8 release). All sequences that failed to cluster when tested against the Greengenes database were used as input for picking OTUs de novo. Representative sequences for the OTUs were Greengenes reference sequences or cluster seeds, and were taxonomically assigned using the Greengenes taxonomy and the Ribosomal Database Project Classifier (Wang et al., 2007). Representative OTUs were aligned using PyNAST (Caporaso et al., 2010b) and used to build a phylogenetic tree with FastTree (Price et al., 2010), which was used to calculate α - and β -diversity of samples using Phylogenetic Diversity (Faith, 1992). Chimeric sequences were identified with ChimeraSlayer (Haas et al., 2011) and excluded from all downstream analyses. Similarly, sequences that could not be aligned with PyNAST, singletons and very low abundant sequences (relative abundance <0.005%) were also excluded.

To correct for differences in sequencing depth, the same amount of sequences was randomly sub-sampled for each group of samples (rarefaction; maximum depth depending on sample group). A bootstrap version of Mann-Whitney-U test was used to compare the diet-dependent or genotype-dependent abundance of OTUs at different taxonomical levels; significant differences were identified after correction for false discovery rate. Abundances higher than 1% are displayed on the genus level. QIIME was used to compute alpha diversity from rarefied OTU tables and to determine statistical significance at maximum rarefaction level by using a two-sample t-test and 999 Monte-Carlo permutations. Beta-diversity and weighted unifracs distance matrix of dietary groups were computed with QIIME and statistical significance of sample groupings was determined by adonis method and 999 permutations.

Quantification of Fermentation Products

Caecal short-chain fatty acids were measured using gas chromatography coupled to mass spectrometry detection (GC-MS) as described previously (Wichmann et al., 2013). Briefly, approximately 20-100 mg of caecal content were mixed with internal standards (Key Resources Table), added to glass vials and freeze dried. All samples were then acidified with HCl, and SCFAs were extracted with two rounds of diethyl ether extraction. The organic supernatant was collected, the derivatization agent N-tert-butylidimethylsilyl-N-methyltrifluoroacetamide (Sigma-Aldrich) was added and samples were incubated at room temperature overnight. SCFAs were quantified with a gas chromatograph (Agilent Technologies 7890A) coupled to a mass spectrometer (Agilent Technologies 5975C).

Western Style Diet Feeding for 0 - 28 Days

11 - 12 weeks old mice fed a chow diet were switched to a Western style diet for 0 -28 days. Mucus properties were examined at the respective days and colonic content was snap-frozen at -80°C for 16S rDNA microbiota analyses as described.

Caecal Microbiota Transplantation

After 10 weeks fed a chow diet mice were gavaged with 200 μ l of an antibiotic cocktail once a day for three consecutive days (ampicillin 1 g/l, metronidazole 1 g/l, vancomycin 0.5 g/l, neomycin 0.5 g/l, Sigma-Aldrich). Subsequently mice were switched to a Western style diet and gavaged weekly with caecal content from age- and gender matched mice fed either a chow diet or a Western style diet. Body weight gain was controlled weekly while metabolic parameters (body fat, fasting glucose, fasting insulin) as well as mucus properties were examined after 6 weeks at the end of the experiment. Colonic content was snap-frozen at -80°C for 16S rDNA microbiota analyses.

B. Longum and Inulin Supplementation

Mice were maintained on a chow diet and switched to a Western style diet at the age of 9 - 11 weeks. Mucus properties were analyzed in a subset of mice (n = 4) to confirm correct physiology of the inner colonic mucus layer before the dietary switch. The remaining mice were divided into 4 groups and fed a WSD for 4 weeks. Autoclaved drinking water was supplemented with 1% oligofructose-enriched inulin (w/v, Orafit Synergi 1, Beneo, Tienen, Belgium), *Bifidobacterium longum* NCC2705 from glycerol stock (about 2 x 10⁶ colony forming units/ml final) or a combination of both and replaced daily. The control group (WSD) received Reinforced Clostridial Medium (Difco) with 20% glycerol but without bacterial cells. Of note, addition of 1% inulin did not alter the amount of viable *Bifidobacterium longum* in the water bottle as compared to control and on average each mouse obtained at least 1.2 x 10⁷ colony forming units per day. Metabolic parameters were analyzed 3 weeks after the dietary switch and mucus measurements were performed after 4 weeks.

QUANTIFICATION AND STATISTICAL ANALYSIS

Statistical analyses have been carried out with GraphPad Prism (version 7.0b) if not stated otherwise in the methods section. For comparisons between two groups an unpaired t-test has been used when samples were distributed normally. For not-normally distributed samples Mann-Whitney U test has been used. In all figures data are presented as mean \pm SEM, except for alpha-diversity (Figures 3B, 3E, 4F, and 5J) where \pm SD is shown. For correlation analysis Pearson correlation coefficients were calculated for normally distributed data while nonparametric Spearman correlations were used for not-normally distributed data. A linear regression line in the figure indicates a significant correlation. For the time course experiment (Figure 4) a linear regression model over time has been used to calculate statistical significance. When comparing 4-5 groups (Figure 6) statistical significance against WSD fed mice (vehicle control) was determined by Kruskal-Wallis test and corrected by Dunn's multiple comparisons test.

All statistical analyses for 16S rDNA sequencing data have been performed with QIIME (Caporaso et al., 2010a) (version 1.9.1). The script *group_significance.py* with a bootstrap version of Mann-Whitney U test with Bonferroni correction has been used to determine statistically significant differences between two groups. For more than two groups (Timepoint experiment; Figure 4) Kruskal-Wallis test has been used. Statistical significance in alpha diversity was determined with the script *compare_alpha_diversity.py* and the default settings (two-sample t-test and 999 Monte-Carlo permutations). Statistical significance in beta-diversity was determined with the script *compare_categories.py* and the adonis statistical method and 999 permutations. Results are presented in Table S1.

DATA AND SOFTWARE AVAILABILITY

The mass spectrometry proteomics data were deposited to the ProteomeXchange Consortium (<http://proteomecentral.proteomexchange.org>). The accession number for the proteomics data reported in this paper is ProteomeXchange: PXD006129. Microbiota 16S rDNA gene sequencing results have been deposited in the ENA sequence read archive (<http://www.ebi.ac.uk/ena/data/view>). The accession number for the microbiota data reported in this paper is ENA: PRJEB20367.